Rochester Institute of Technology

RIT Digital Institutional Repository

Theses

5-6-2024

Electron Counting, Dopant Implementation, & Electron Phonon Interaction Mesh Sensitivity Testing for Nanoscale Energy Transport Model

Dominick Velez
dv5299@rit.edu

Follow this and additional works at: https://repository.rit.edu/theses

Recommended Citation

Velez, Dominick, "Electron Counting, Dopant Implementation, & Electron Phonon Interaction Mesh Sensitivity Testing for Nanoscale Energy Transport Model" (2024). Thesis. Rochester Institute of Technology. Accessed from

This Thesis is brought to you for free and open access by the RIT Libraries. For more information, please contact repository@rit.edu.

Rochester Institute of Technology

Master's Thesis

Electron Counting, Dopant Implementation, & Electron Phonon Interaction Mesh Sensitivity Testing for Nanoscale Energy Transport Model

Dominick Velez

Thesis Committee:

Dr. Michael P. Medlar

Dr. Santosh K. Kurnick

Dr. Martin K. Anselm

Defense Date: May 6, 2024

A Thesis Submitted in Partial Fulfillment of the Requirements for the Degree of Master of Science in Manufacturing and Mechanical Systems Integration

Department of Manufacturing and Mechanical Engineering Technology

College of Engineering Technology

Abstract

Managing thermal energy generation and heat transfer within nanoscale devices (transistors) of modern-day electronics is important as it limits speed, carrier mobility, and affects device reliability. In the nanoscale, heat conduction occurs primarily via phonon transport and heat generation is a result of electron-phonon interactions in these devices. Traditional methods of predicting physical behavior have proven to lack either physical accuracy, computational efficiency, or flexibility. The Nanoscale Energy Transport Model (NETM) is an engineering design tool introduced to calculate non-equilibrium transport of energy carriers in nanoscale devices and overcome the deficiencies of traditional models of energy-carrier transport The NETM previously had a rudimentary model to represent heating from electron-phonon interactions. This thesis builds a foundation for a more detailed representation of the transport and interaction of electrons and phonons with three major goals. First, to create a method of calculating equilibrium energy carrier concentrations across the first conduction band electronic structure for a silicon lattice and implement it into the NETM. Second, to create a preliminary model to calculate the effect of N-type dopant on the energy carrier concentration within the silicon lattice. And third, to do a wavevector space mesh sensitivity on the possible electron-phonon interactions subject to energy and momentum selection rules. The model implementation results compare well to similar methods in the literature. This forms the basis of the implementation of Fermi's golden rule for the electron-phonon scattering rate computation and can lead to a full joule heating model.

Acknowledgements

First and most importantly, I wish to thank my father, mother, and sister for their never-ending support for me and my endeavors. They have always been there and supported me on my most dower of days and always gave me the support to continue. Special thanks to my mother for listening in on my never-ending rambles about electron-phonon interactions and attempting to understand my ideas, no matter how abstract.

I would like to express my sincerest gratitude to Dr. Medlar for the willingness to be my advisor during the entire process of composing this thesis. The growth of my interest in the nanoscopic world can be attributed to his teachings. Along with this, I express even more gratitude to assisting me in refining my ability to write and process my thoughts and observations throughout the thesis process. I thank him for his support.

A big thank you to Dr. Kurnick for assisting me in understanding more about solid state physics. The assistance she provided was invaluable for understanding electron transport and transistor design principles.

Thank you to Dr. Martin K. Anslem for taking the time out of his busy day to review this work and provide constructive feedback to improve and refine my work and continued advancement into the academic world.

Table of Contents

Abstract 2
Acknowledgements 3
List of Figures 6
Introduction 10
Transistor Devices, Silicon Structure, & Heat Transport 10
Traditional Modeling Approaches 13
Convection and Conduction Paired Models (Macroscale Models) 13
Macroscale Model Shortcomings 15
Nanoscale Energy Transport Model (NETM) 16
Current NETM Shortcomings 17
Objectives 17
Literature Review and Theory Background 18
Nanoscale Heat Conduction 18
Lattice Structures and Electrons 18
Electron Populations in Transistors 21
Density of States Theory 25
Dopant and Fermi level shifting 31
Phonons & Three Phonon Scattering 34
Electron and Phonon Interaction Scattering and Heat Generation 41
Modeling Implementation 42
Methodology 42
Electron Population 43

Dopant Charge Carrier Contribution Population Initial Implementation 45

Electron Phonon Mesh Analysis 46

Validation and Modeling Results 47
Comparisons to Published Literature 47

Rowlette and Goodson Simulations 47

Jin and Fischetti 48

Martin and Gonzalez: One Dimensional Electron Transport Analysis 48

Ashraf: Intrinsic Carrier Concentration in Presence of Degenerate Doping 49

Results Discussions 50
Density of States 50

Dopant Correlation Results 51

Mesh Sensitivity Results 52

Summary, Conclusions, and Future Work Recommendations 54
Summary 54

Conclusions 55

Future Work Recommendations 55

References 58

List of Figures

Figure 1: Microchip transistor sizes from 2000 to 2020. Reproduced from [1]. 10

Figure 2: Number of Transistors Per Computational Device, Reproduced From [2] 11

Figure 3: Microprocessor Trend Data, Reproduced from [3]. 12

Figure 4: A diagram of a MOSFET transistor with its heat flow represented as a red arrow. The dimensions of the transistor are H, D, W, and L. L being the gate length, D being the total depth of the transistor, H being the height of the transistor, and W being the width of the transistor. The directional coordinates of which is shown using a i, j, and k coordinates system to represent the basis vectors in the x, y, and z directions, respectively. 14

Figure 5: Convection from microchip to a fluid showing a transistor as the most basic source of heat generation, not to scale. Adapted from [5] 15

Figure 6: Face Centered Cubic diamond structure. Reproduced from [15]. 19

Figure 7: $3p_x$ and $3p_z$ orbitals.in silicon. Each orbital is oriented along its designated axis. Reproduced from [17]. 21

Figure 8: The one-dimensional Kronig-Penny model, each barrier represents the gaps between the ion cores and each well represents the ion cores themselves. 22

Figure 9: The solution curve to the Kroing-Penny model. The x-axis represents the periodic energy of the lattice spacing and the y-axis represents the wavevector possibilities. Reproduced from [14]. 22

Figure 10: Depiction of band gap Structures for Metal, Semiconductor, and Insulator Materials. The blue bar represents the valance band, and the orange bar represents the conduction band. [14] 24

Figure 11: E-k Diagram of silicon across different lattice directions in momentum space across different allowable wavevectors. Reproduced from [20]. 24

Figure 12: 3D Density of States across the energy spectra. Reproduced from [14]. 27

Figure 13: Bose-Einstein, Maxwell-Boltzmann, and Fermi-Dirac Statistics as Compared across the energy spectrum with ε being the energy of the particle, μ being the chemical potential, k_b being the Boltzmann constant, and T being the overall system temperature. Reproduced from [21]. ... 29

Figure 14: The Fermi distribution at a range of temperatures. ... 30

Figure 15: Fermi Distribution at Shifted Fermi Levels ... 30

Figure 16: Visual of dopant introduced into the lattice. The right image shows pure silicon without any added dopant while the right image shows two cases: P-Type (Boron doped silicon with extra vacancies "holes" in the lattice) and N-Type (Antimony doped silicon with extra valance electrons). Reproduced from [22]. ... 32

Figure 17: A depiction of band gap narrowing within a semiconductor device. Once enough dopant has been introduced into the lattice of the material, the bandgap will begin to narrow. This leads to more metallic like electrical conductivity within the semiconductor. Reproduced from [24] ... 33

Figure 18: 1-D Toy Model of an Atomic Chain ... 34

Figure 19: Parabolic Potential Curve and Its Associated Energy Modes with the overlayed wavefunction for each energy level. Sourced from [26]. ... 35

Figure 20: Dispersion Relationship of a 1-D Monatomic Chain, with a representing the lattice spacing between the individual atoms. [19] ... 36

Figure 21: First Brillouin Zone of Silicon, Reproduced from [5]. ... 37

Figure 22: Image of Acoustical and Optical Modes ... 37

Figure 23: Experimental Values for Silicon Dispersion in the (100) Direction at 300 K. Triangles Are Data from Nilsson and Nelin [29], Open Circles Are from Dolling [30]. ... 38

Figure 24: Illustration of 1-D three phonon scattering where ks' and k's' combine to produce k"s", Type II reverse the order. Adapted from [5] ... 39

Figure 25: Normal vs. Umklapp three phonon scattering in a 2-d representation of the wavevector space. Phonons K1 and K2 interact to result in vector K3 in the normal process on the left. Phonons K1 and K2 interact to result in K3 that is reflected back into the FBZ with the reciprocal vector G in the Umklapp process on the right. Reproduced from [5]. 40

Figure 26: Electron-phonon interaction Feynman diagram. The $e-$represent the electrons and the arrows represent the states with the black arrows are the initial states and the orange arrows represent the final states. The wave k, s represents the phonon interaction of emission and absorption form one electron to its local neighbor........ 42

Figure 27: Visual guide for modeling approach and steps. Solid lines represent work done; dashed lines represent future work to be done. 43

Figure 28: A depiction of the states located along the conduction band. Each state at the conduction band will exist among a dk interval in dE energy range. As such, a relationship between dk and dE can be used to find all the states located along the interval. 44

Figure 29: Schematic illustration of the one -dimensional domain simulated by Rowlette and Goodson [13]. 47

Figure 30: Schematic of a gated nanowire structure that was considered under the Jin and Fischetti Study [31]........ 48

Figure 31: Bulk Silicon wire model used in Martin and Gonzalez [32]. 49

Figure 32: Dopant Electron Element Occupation Locations across the energy spectra. The results for the 3mm diameter wire from Jin et al [31] are shown as the red line. 50

Figure 33: E-K Diagram results for the new model, with the NETM results represented in the blue circles, Rowlett et al [13] is represented in red, and Martin et al [32] is represented in yellow. 51

Figure 34: Dopant relationship to dopant proportionality........ 51

Figure 35: NETM Algorithm comparison with Ashraf [34]. The blue line represents the NETM algorithm predictions while the red circles represent data from Ashraf. 52
Figure 36: Mesh Sensitivity Test Histogram Relating Energy Values vs Interaction Count 53
Figure 37: Mesh Sensitivity Test Histogram Relating Energy Values vs Interaction Count 53

Introduction

Transistor Devices, Silicon Structure, & Heat Transport

Thermodynamics within nanoscale electronic devices (transistors, operational amplifiers, etc.) of modern microelectronics is an important design consideration as increased temperature can lead to device degradation, limits on maximum device performance, and failure. Elevated temperatures can degrade performance due to decreased carrier mobility in the device and interconnect resistivity at device junctions. This can lead to device failure and reliability issues when used for an extended period of time. This is mostly related to the continued scaling of transistors sizes over time, as transistors become smaller and smaller thermal management becomes a more prevalent problem due to transistor density. Data for microchip transistor sizes is shown in figure 1.

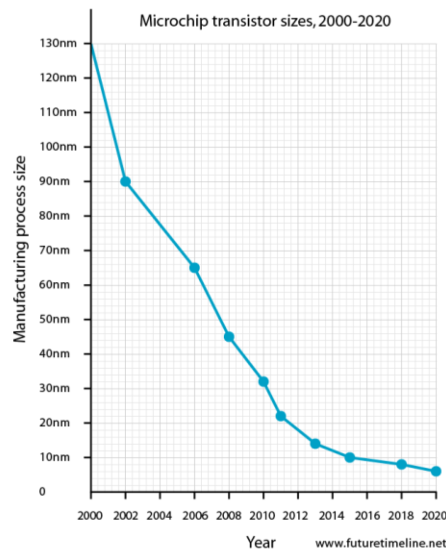

Figure 1: Microchip transistor sizes from 2000 to 2020. Reproduced from [1].

Data on the number of transistors in a processing device on average are shown in figure 2.

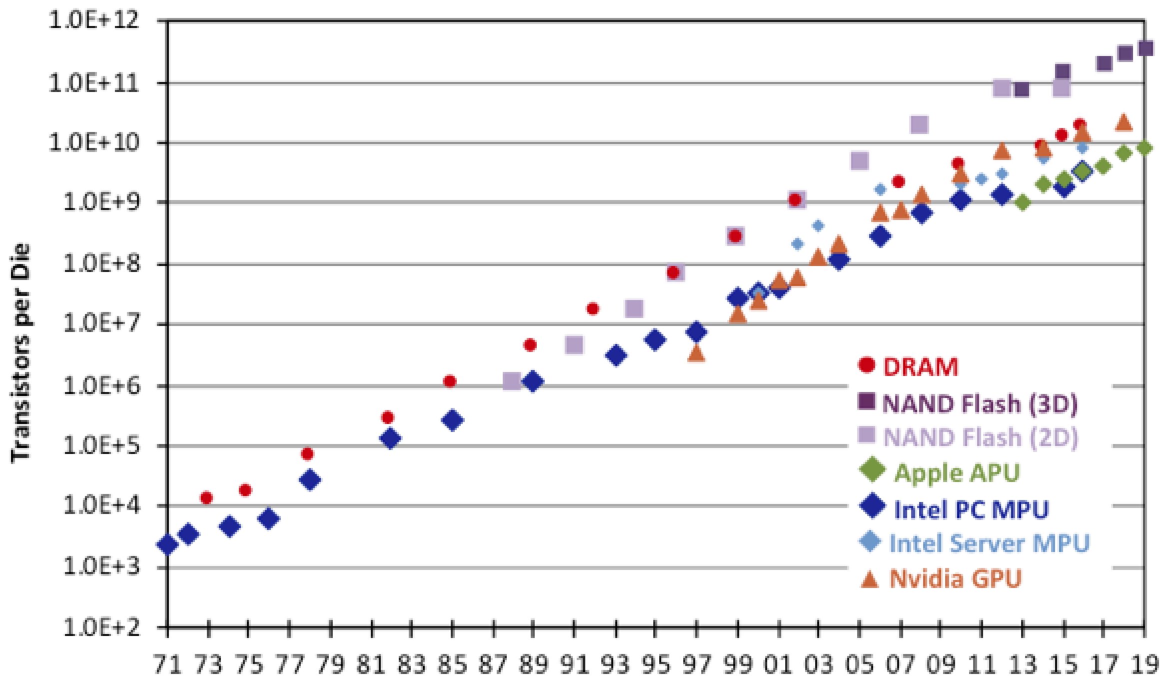

Figure 2: Number of Transistors Per Computational Device, Reproduced From [2]

As shown, the transistor count in current semiconductor CPUs has already passed one-billion transistors. This is in line with the concept of Moore's Law, the observation that the number of transistors within an integrated circuit has doubled each year. This is also better illustrated by the data compiled by Karl Rupp [3] as shown in Figure 3.

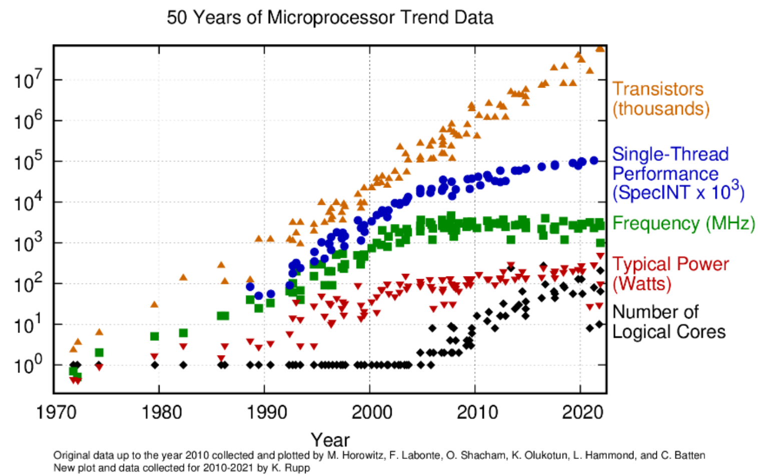

Figure 3: Microprocessor Trend Data, Reproduced from [3].

Figure 2 shows that with the number of transistors increasing, the Single-Thread performance, frequency, and typical power have tapered off since the early 2000's. The most significant of these data trends that have been tapered off is the frequency, as its limitations in modern processors allow for decreased thermal performance degradation if designed and accommodated correctly. This is due to the direct correlation between heat generation and frequency, as the more frequency is increased the more heat is generated in the device due to the higher movement of charge carriers. Many engineering tools attempt to solve this problem by predicting heat transfer at the microlevel using assumptions and macroscale heat equations. However, due to the fundamental issues of translating macroscale effects to the nanoscale, these calculations are often imprecise. And attempts at direct atomic simulation often are incredibly computationally intensive. ANSYS, one of the most widely used computational tools, requires a use of eight gigabytes of ram per CPU core to run efficiently for their direct atomic simulation suite [4]. The Nanoscale Energy Transport Model, developed by Dr. Michael Medlar, allows for a less hardware intensive tool suite for heat generation calculations due to its flexibility, efficiency, and accuracy for calculating phonon dispersion within silicon lattices [5]. This is due to the consideration and combination of techniques used in quantum mechanics,

improvement upon established Monte-Carlo simulation techniques, and basic statistical mechanics. The goal of the Nanoscale Energy Transport Model [5] is to fill the gap and meet the needs of engineers and designers to allow more efficient computation of heat generation within semiconductor devices while maintaining accuracy and low processing time.

Traditional Modeling Approaches

This dissertation deals with the modeling of heat transfer associated with modern transistor geometries. The primary mechanism of heat transfer within solid devices, such as transistors, is conduction. A brief review of the general macroscale type models used to predict conduction and other mechanisms of heat transfer will be presented. The shortcomings of these models (primarily macroscale conduction) at nanoscale sizes and picoseconds time scales will be discussed briefly as the motivation for different modeling approaches.

Convection and Conduction Paired Models (Macroscale Models)

Heat conduction is the transport of heat within a medium where there is no bulk motion of atoms or molecules in the medium [6]. Macroscale condition is modeled with Fourier's law of heat conduction, which states that the rate of heat transfer through the given material is proportional to the negative gradient of the temperature across the medium. To represent this mathematically, the gradient function is used as shown below in equation 1.

$$\frac{dq}{dt} = -k\nabla T \tag{1}$$

Where $\frac{dq}{dt}$ is the rate of heat transfer, k is the thermal conductivity of the given material, and ∇T is the temperature gradient across the x, y, and z directions. If we are only considering a one-dimensional case, then the equation simplifies to the following as equation 2.

$$\frac{dq}{dt} = -kA\frac{dT}{dx} \tag{2}$$

Where A is the cross-sectional area of the material being analyzed and $\frac{dT}{dx}$ is the gradient across the x-direction only. Combining this with conservation of energy creates the equation for heat conduction, where transient thermal responses can be predicted across many macroscale scenarios. Equation 3 shown below is this equation for the one-dimensional case with isotropic (same properties across all dimensions) thermal conductivity [6].

$$k\frac{\partial^2 T}{\partial x^2} + \frac{\partial q}{\partial t} = \rho C\frac{dT}{dt} \tag{3}$$

Where $\frac{\partial q}{\partial t}$ is the volumetric heat generation rate, ρ is the density of the material and C is the specific heat (for an incompressible fluid or solid, $C = C_v = C_p$). In relation to transistor devices, the heat flow can be modeled as the heat traveling across the x-direction from source to drain. A visualization of this is shown below in figure 4.

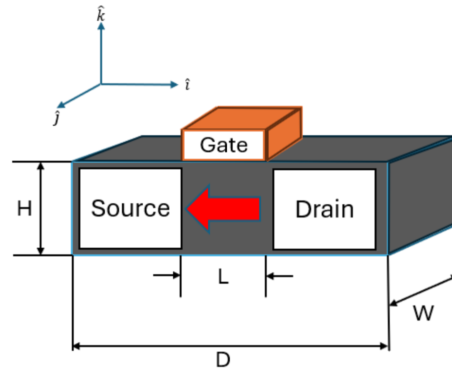

Figure 4: A diagram of a MOSFET transistor with its heat flow represented as a red arrow. The dimensions of the transistor are H, D, W, and L. L being the gate length, D being the total depth of the transistor, H being the height of the transistor, and W being the width of the transistor. The directional coordinates of which is shown using a $\hat{\imath}$, $\hat{\jmath}$, and $\hat{k}$ coordinates system to represent the basis vectors in the x, y, and z directions, respectively.

Convection, in contrast, deals with the transfer of thermal energy between the hot and colder fluid medium by the bulk motion of molecules of the fluid medium [6]. This involves the process of conduction to the

fluid in the immediate vicinity of the surface and the movement of the fluid away from the surface carrying the heat away from the surface. Bulk motion can occur though either density variations in the fluid (buoyancy driven flow) or though externally forced fluid motion. For a simple integrated circuit chipset (IC) this is illustrated with figure 5.

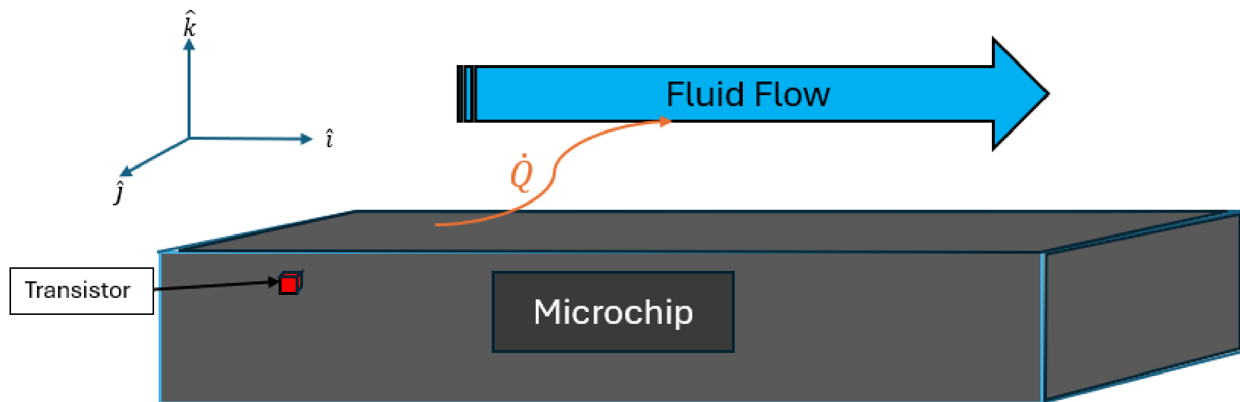

Figure 5: Convection from microchip to a fluid showing a transistor as the most basic source of heat generation, not to scale. Adapted from [5]

To predict convective heat transfer across a surface, predictions of the fluid conditions adjacent to the microchip are required. That is typically done by using three governing equations for conservation mass, momentum, and energy. The three equations are formulated for a differential control volume and using simultaneous equations, can be solved to predict heat transfer from the surface of the microchip.

Macroscale Model Shortcomings

Due to macroscale limitations, Fourier's law of heat conduction becomes unreliable at nanometer and sub nanometer length scales and picosecond time intervals [7,8]. This occurs due to the breakdown of local thermodynamic equilibrium at the length scales of current modern day semiconductor devices. The assumption that implies that the local temperature is an accurate representation of the distribution of phonons in the medium that is being observed. The assumption becomes invalid at the length scales and time scales of modern-day transistors due to approaching the mean free path and scattering time of the dominant energy carriers in the device [9]. For silicon (depending on the temperature distribution), the

representative values of the mean free path and scattering times range from 100nm – $1\mu m$ and 10 ps – 10 ns respectively [10]. According to figure 1, transistor feature sizes have well surpassed this limit since the early 2000's. In addition, transistor frequencies have long since surpassed the characteristic scattering times in a similar time period. Intel® with their new Core™ Alder Lake™ architecture can allow for boost frequencies up to 6.0 GHz in transistor switching in near 2 nanosecond switching times in their I9 line of products [11]. This indicates that the future of transistor type technologies will be far outside the scope of Fourier's law. Thus, there is a huge demand for the direct simulation and modeling of transport of energy carriers across a variety of device platforms to track thermal energies. In semiconductors, the dominant thermal energy carrier is the phonon, and the primary mechanism of joule heating is the electron-phonon interaction. As such, nanoscale simulations are more appropriate to model these types of behaviors in transistors and other semiconductor devices.

Nanoscale Energy Transport Model (NETM)

The Nanoscale Energy Transport Model (NETM) [5] is a quasiparticle approach to modeling energy carrier interactions and transport. The first iteration of the NETM was called Statistical Phonon Transport Model (SPTM) and only modeled phonon transport and interactions. The modeling approach of the SPTM and thus the NETM consists of the following: First, the NETM creates the real lattice space and using the Fourier transform transforms the space into the wavevector space and meshes the newly created space. Second, using lattice dynamics, computes the phonon dispersion across the meshed wavevector space. Third, it searches across the meshed wavevector space to find the allowable three phonon interactions based on conservation of energy and momentum selection rules. Fourth, utilizing Fermi's golden rule it computes the scattering rates of the each allowed interaction for three phonon scattering. And finally, it updates the entire phonon populations at each iterative timestep based on the results of scattering and real-space drift based of the phonon group velocity. Heat generation is as result of the electron-phonon interactions and is

treated as an input parameter that results in a phonon generation rate. The spectrum of phonon generation is based off limited studies of electron phonon interaction densities.

Current NETM Shortcomings

The treatment of the interactions between phonons and electrons in the current implementation of the NETM is a shortcoming that limits model accuracy. The electron-phonon scattering rate, as described in Fermi's Golden Rule is not computed directly. The volumetric heat generation rate, which is a consequence of interactions, is treated as a geometric cell input parameter. At each time step, the energy input to each cell is computed as the product of the heat generation rate, the cell volume, and the discrete time step. The cellular energy input results in a net production of phonons, but not all phonon modes create phonons at the same rate per time step. The spectrum of phonon generation depends on the phonon wavevector, frequency, and polarization. The static spectrum was computed using two parameters, the electron-phonon scattering strength and the electron-phonon interaction density, respectively. The scattering strength parameter is based on the different deformation potentials from different phonon modes. And the interaction density was estimated using a 1-dimensional approximation. A fit to the phonon dispersion in the (100) direction and a parabolic conduction band model was used to compute allowable electron-phonon interactions (Rowlette and Goodson model) [12]. With the limits of momentum and energy conservation imposed.

Objectives

The goal of this thesis is to address the shortcomings of the representation of electron-phonon interactions in and assist in creating the foundation for a full electron-phonon scattering model for bulk silicon transistor-based devices. This consists of the following steps:

1. Initialize the electron population within the conduction band allowing for consideration of both doped and intrinsic charge carriers.

2. Understand the proportionality of dopant vs. the number of electrons present above the conduction band by using a first order model.
3. Investigate the mesh sensitivity of the wavevector space element size to the electron-phonon interaction statistics.

Literature Review and Theory Background

Nanoscale Heat Conduction

At the nanoscale level, conduction can be thought of as the result of two distinct mechanisms. These mechanisms consist of the movement of electrons in the lattice of the selected material and the transport of energy associated with the vibrational waves in the lattice [10]. Within semiconductors, both mechanisms are prevalent for the discussion of heat transfer with phonons representing the majority of heat carriers and their interactions with energy carriers changing some of their key characteristic values: energy and momentum.

Lattice Structures and Electrons

A crystal structure is the periodic arrangement of atoms in a crystal which can be described mathematically as a lattice, an identical and infinite array of points in space where the neighboring points are identical to all others [13]. The most basic unit of the crystal lattice is called the unit cell. For silicon, the unit cell is a face centered cubic diamond structure where the atoms occupy the faces of the cube. A visual of this is shown below in figure 6.

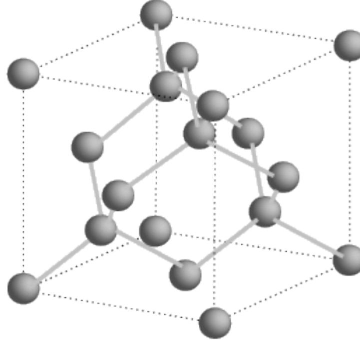

Figure 6: Face Centered Cubic diamond structure. Reproduced from [15].

To understand these structures and their formations, an understanding of the electron's behavior must be known as to understand the population dynamics and orientations of the charge carrier.

In quantum mechanics, electrons are the most fundamental charge carrier particle. As such they are the primary conduction energy carriers in a semiconductor. All quantum particles can be treated as waves due to wave/particle duality; this means that the fundamental particle can act as a wave and be predicted using wave mechanics [16]. For electrons, a fundamental relationship is the frequency energy relationship. This is given by the following equation:

$$\mathrm{E} = \hbar|\vec{\omega}| \tag{4}$$

Where E is the total energy of the particle, $\hbar$ is the half Planck constant which is given in the amount of $1.0574718 * 10^{-34}$ J-s, and $|\vec{\omega}|$ being the magnitude of the angular frequency vector given in radians per second. Another useful descriptor of a quantum particle is the momentum of the particle. This is also described by the following equation:

$$\vec{p} = \hbar\vec{k} \tag{5}$$

Where $\vec{p}$ is the momentum of the traveling particle and $\vec{k}$ is the wavevector in units of radians per meter. The wavevector describes the spatial frequency and direction of the traveling particle.

The electron, due to the nature of wave-particle duality which is governed by the Schrodinger's equation [14,16,17]. Schrodinger's equation gives the complete time and energy description of the particle under analysis. It can be written as such:

$$i\hbar \frac{\partial \Psi}{\partial t} = \hat{H}\Psi \quad (6)$$

Where i is the imaginary number, Ψ is the wavefunction of the particle that give the complete description of the particle's states, and $\hat{H}$ is the Hamiltonian of the particle. The Hamiltonian is the complete energy description of the particles state and is often given in the form of:

$$\hat{H} = \hat{T} + \hat{V} \quad (7)$$

Where $\hat{T}$ is the kinetic energy and $\hat{V}$ being the potential energy.

Solving for this equation gives rise to the idea that electrons will have a preference of where they can and cannot be found depending on the potential coulombic interaction and the kinetic energy. This leads to the rise of the idea of orbitals, locations surrounding the atom where there is a higher probability that an electron will be found. These orbitals are what give structure to the atom when there is an interaction between two nearby neighboring atoms. For semiconductors, this leads to the structure of silicon being very orderly due to the fact that in silicon. This is due to there are two free electrons out of the fourteen that is attached to the nucleus that can be paired in silicon's outer most electron shell (called the p shell), $3p_x$ and $3p_z$. A depiction of these electron orbital shells is shown below.

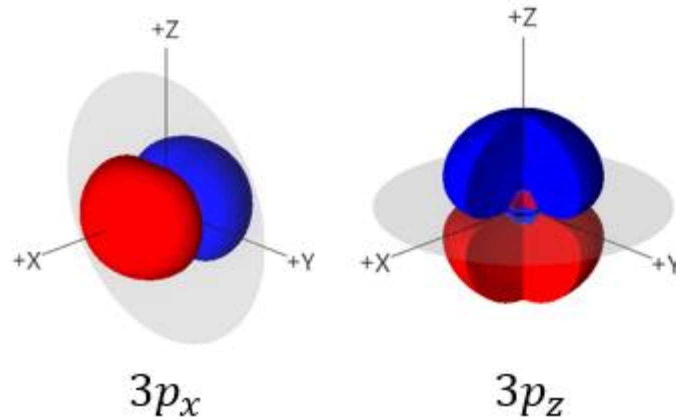

Figure 7: $3p_x$ and $3p_z$ orbitals.in silicon. Each orbital is oriented along its designated axis. Reproduced from [17].

These specific orbitals lead to the consequences of crystal structures. As crystal structure is the periodic arrangement of atoms in a crystal, the periodicity leads to periodic interacting coulombic interactions. This leads to the effects of bands and periodic potentials, which affect the electron position and populations across the silicon lattice.

Electron Populations in Transistors

Electrons within solids are bounded to certain states due to the nature of quanta within the nanoscale regime [14,16,17]. Once many atoms are introduced in a regular lattice pattern, a more intricate approach must be taken for solving for the electrons wave function as instead of being bound to a simple atomic core, many of these cores are connected in a regular pattern to each other. Each of these core's act as a potential barrier that the electron must overcome to go across the lattice. For a simplified model, the one-dimensional case can be considered where the electrons are going across this one-dimensional chain of wells and barriers. The formal definition of this model is the one-dimensional Kroing-Penny model [14], a picture of which is shown below in figure 8.

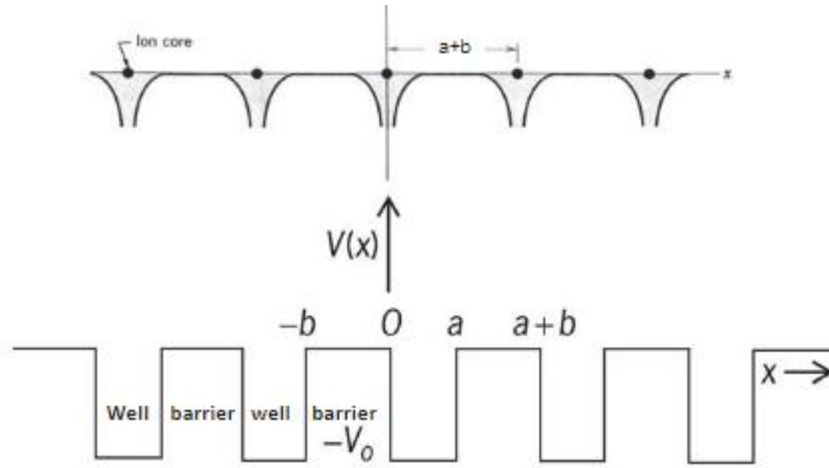

Figure 8: The one-dimensional Kronig-Penny model, each barrier represents the gaps between the ion cores and each well represents the ion cores themselves.

To solve this situation for the electrons wavefunction, a theorem known as Bloch theorem is used. The Bloch theorem states that the eigenstates of the Hamiltonian can be chosen to have the form of a plane wave times a function with the periodicity of the Bravais lattice (the most basic unit cell of a lattice) [16,18,19]. Mathematically, the way to represent this is using equation 8 below:

$$\psi(\vec{r} + \vec{R}) = e^{i\overrightarrow{kR}}\psi(\vec{r}) \tag{8}$$

Where $\vec{R}$ is the lattice vector of the Bravais lattice. Using this and solving for the wavefunction using Schrodinger's equation gives a relationship between the well and barrier regions. Solving for the relationship gives a graph that follows a sinusoidal decaying curve. This is shown below in figure 9.

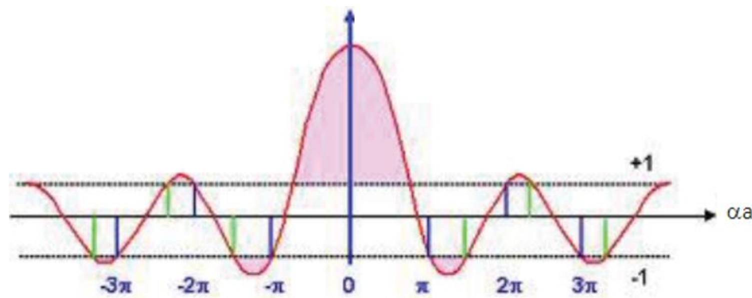

Figure 9: The solution curve to the Kroing-Penny model. The x-axis represents the periodic energy of the lattice spacing and the y-axis represents the wavevector possibilities. Reproduced from [14].

Looking at the curve, the only possible solutions that are valid to solve for are the values between 1 and -1 due to those values representing the valid states of electron existence. This solution leads to a banding effect due to the strong coulombic forces exerted by atoms being regularly spaced [14,18]. This (as described in solid state physics) leads to a banding effect as described by a theory called the band theory of solids.

The band theory of solids says that due to the fact that there are N number of many atoms occupying a given space, and the consequences of the atoms being regularly spaced together in the solid, the energy locations where certain electrons occupy are described by bands [16]. These bands occur due to the discrete energy levels where electrons are able to occupy (the electron orbitals) start to layer upon each other creating a continuum. There can be numerous energy bands depending on the solid and its characteristics. However, the most important energy bands that most engineering applications are concerned with are the valance band, conduction band, and the forbidden band. The valance band is the band below the conduction band but the electrons at this band are loosely bound to the atom's nucleus. The conduction band is the energy band where electrons are considered "free" and no longer localized around the nucleus of a given atom. The forbidden band (sometimes referred to as the band gap) is the energy gap between the valance and conduction band [14,16,18]. The band gap determines the electrical conductivity of the material with which we are working. In solid state theory, three types of solids are often characterized by this type of band gap relationship: metals, semiconductors, and insulators. Metals have many states and bands, to the point where the valance and conduction bands begin to touch and, in some cases, overlap. Semiconductors exhibit a bandgap but can have this gap closed with an applied voltage. This is the reason transistors exhibit the behaviors that they do, as the band gap is able to close and allow energy carriers to travel across the source to the drain. Insulators have the property of having an incredibly wide bandgap. So wide that electrical conductivity requires an enormous amount of volage applied across the material substrate [14,16]. A diagram of all of these material band gaps is shown below:

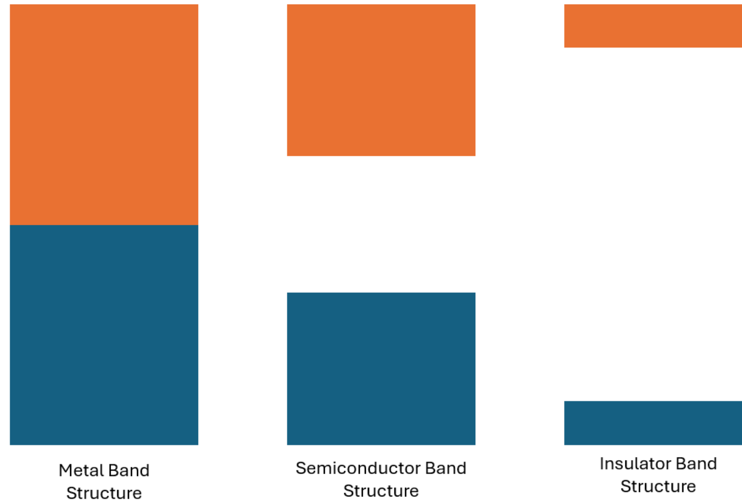

Figure 10: Depiction of band gap Structures for Metal, Semiconductor, and Insulator Materials. The blue bar represents the valance band, and the orange bar represents the conduction band. [14]

However, due to the fact that crystal orientation can affect properties of charge transport, the gap between the conduction band and valance band is also different depending on the orientation axis. In wavevector space, the model for these differences in conduction and valence band energy is plotted on a graph called the E-k diagram, where k is the wavevector depending on the orientation and E is the energy in electron-volts. Figure 14 shows the E-k diagram of silicon.

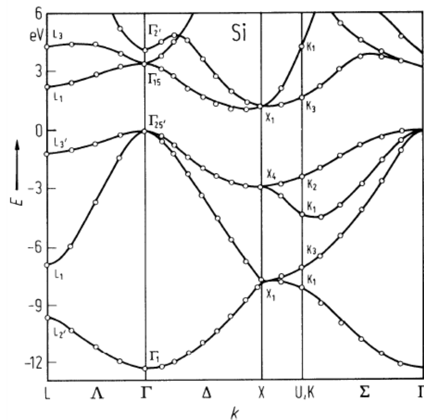

Figure 11: E-k Diagram of silicon across different lattice directions in momentum space across different allowable wavevectors. Reproduced from [20].

To understand how many electrons populate a certain band two equations known as the density of states function and the probabilistic occupation function are used in conjunction to calculate the electron populations.

Density of States Theory

In solid state theory, we need to understand how many states are available to fill within the lattice of the structure we are observing for energy carrier transport [19]. Usually, within a one or two atom system, this is done by the Pauli exclusion principle and the use of molecular orbital theory to understand where the electron is filling in the state and how many states are available to be filled. However, once a many-body electronic system is introduced, it is not accurate to state a one-to-one jump transition of a box. As with banding theory, the electron now has many possibilities of where it could land given the overlapping of states within a given volume [14,16,18]. The density of states theory, however, is used for this purpose. A density of states function tells us the number of available states in a given energy range for an energy carrier to occupy. Along with a function of probability, the combination allows a description for how many particles are being filled at a certain state. For example, a free electron confined within a bulk three-dimensional can be modeled as a quantum particle in a three-dimensional box [14]. To make this situation applicable to find the momentum, an understanding of the relationship of the lengths and wavevectors must be obtained. This is however trivial, using a simple relation an understanding of this relationship can be understood in equation 9.

$$k = \frac{2\pi}{\lambda} \tag{9}$$

Where λ is the wavelength of one period of the wave in meters. If all the lengths are assumed to be the same to find the amount of volume occupied in momentum space, we use the relation shown in equation 15.

$$(\Delta k)^3 = \Delta k_x \Delta k_y \Delta k_z = \frac{2\pi}{L_x}\frac{2\pi}{L_y}\frac{2\pi}{L_z} = \frac{(2\pi)^3}{L^3} = \frac{(2\pi)^3}{\Omega} \tag{10}$$

With Ω representing the phase space volume (momentum space volume) that the wavevector $\vec{k}$ can travel. With that, we can find the number of total states by dividing the total amount of momentum space available to the electrons with the amount of volume occupied in momentum space, as shown in equation 16 [14].

$$N = \frac{2 * 2\pi k^2 dk}{\frac{(2\pi)^3}{\Omega}} \tag{11}$$

And to find the density of states, we can use the base energy of the particle (often called the ground state energy) and use the energy per wavevector to solve as shown in equations 26-29 [14].

$$k^2 = \frac{2mE}{\hbar^2} \tag{12}$$

$$dk = \frac{dE}{\frac{dE}{dk}} = \frac{dE * m}{\hbar * \sqrt{2mE}} \tag{13}$$

$$N = \Omega * \frac{8\pi}{(2\pi)^3} * k^2 * \frac{dE * m}{\hbar * \sqrt{2mE}} \tag{14}$$

$$g(E)dE = \frac{1}{2\pi^2}\left(\frac{2m}{\hbar^2}\right)^{3/2} \sqrt{E}dE \tag{15}$$

Equation 12 is the energy and wavenumber relationship for a simple electron existing within a three-dimensional box. Equation 13, then gives us the more general relationship involving both energy and the energy derivative in respect to wave space. That allows the observation of the direct energy dependency upon each discretized portion of k-space. 14 is the recognition that to account for all the states within the solid, we must take the total phase space volume and multiply it by the probabilistic potential of an electron

existing at that place. Finally, 15 is diving N by the phase space volume Ω to obtain a density of states (how many states there are in the solid) function. A graph of equation 24 is shown below in figure 12.

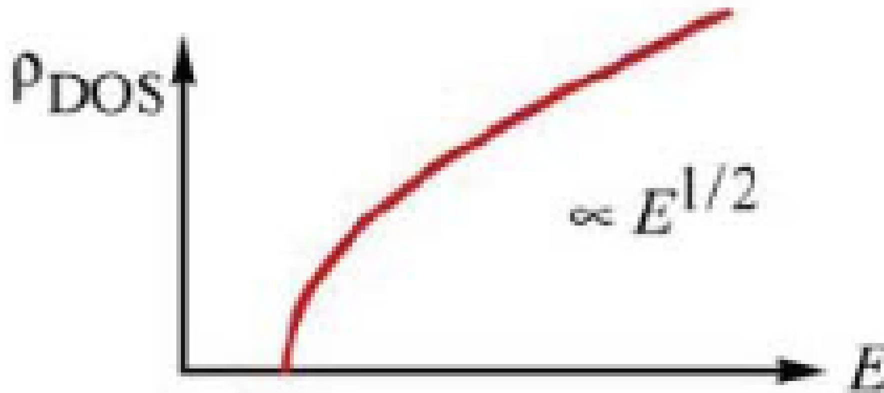

Figure 12: 3D Density of States across the energy spectra. Reproduced from [14].

However, in a general case of a solid of a more complex periodic potential we can use the following relation to understand the relationship of the number of particles to the density of states in equation 16:

$$N(E)dE = g(E)f(E)dE \tag{16}$$

Where $N(E)$ is the number of particles per unit volume between energy E and $E + dE$, $g(E)$ is the density of states function, and $f(E)$ is the distribution function or the probability function that a particle exists in energy state E. For counting the total sum of all the number of electrons existing across all energy bands, we can take equation 16 and integrate it across all energy bands available as shown in equation 17.

$$e_{\#}^{-} = \int_E N(E)dE = \int_E g(E)f(E)dE \tag{17}$$

In particular interest is the function $f(E)$ as it tells us the probability of a particle occupying a particular band. This is determined by either Fermi-Dirac, Bose-Einstein, or Boltzmann statistics [21]. Fermi-Dirac statistics describe the statical probability that a fermion is distributed among a set of energy states. Fermions have the properties of being indistinguishable, obeying the Pauli exclusion principle, having odd-half integer

spin, and their wavefunctions can overlap. Electrons obey these principles, and as such the Fermi-Dirac distribution is used to describe them. The equation for Fermi-Dirac statistics is shown below in equation 18 [21].

$$f_{Fermi}(E) = \frac{1}{1 + e^{\frac{E-E_f}{k_b T}}} \tag{18}$$

Bose-Einstein statistics describe the statical probability that a boson is distributed among a set of energy states. Bosons have the properties of being indistinguishable from each other, they do not obey the Pauli exclusion principle, have whole integer spin, and their wavefunctions can overlap. Phonons obey these principles due to being a quasi-particle and not having any type of spin associated with them. The equation for this statistic is shown in equation 19 [19, 21].

$$f_{BE}(E,T) = \frac{1}{e^{\frac{E}{k_b T}} - 1} \tag{19}$$

When the population becomes noticeably big, they begin to converge to another type of distribution known as the Maxwell-Boltzmann distribution. This distribution accounts for particles that are identical to each other but can be sorted and distinguished depending on the order, have any type of spin characteristic, and their wavefunctions do not overlap. Some examples of this behavior are gas molecules or many high energy bosons. The equation for Maxwell-Boltzmann distribution is shown below in equation 20.

$$f_{MB}(E) = e^{-\frac{E-E_f}{k_b T}} \tag{20}$$

For a visualization of both statistics compared to regular Boltzmann statistics is shown in figure 13.

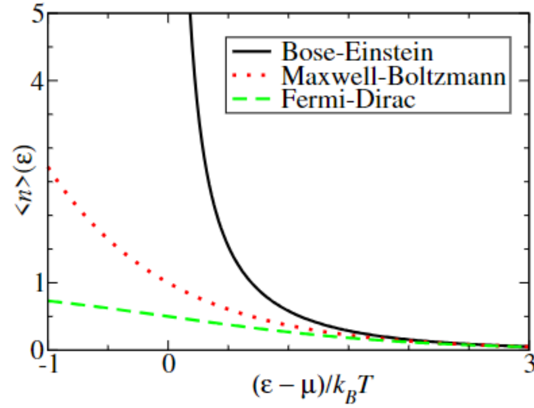

Figure 13: Bose-Einstein, Maxwell-Boltzmann, and Fermi-Dirac Statistics as Compared across the energy spectrum with ε being the energy of the particle, μ being the chemical potential, k_b being the Boltzmann constant, and T being the overall system temperature. Reproduced from [21].

With each of these statistics there are two dependencies, the temperature of the system and the chemical potential. In solid state physics, our chemical potential is the Fermi level of the system. The Fermi level is the term used to describe the top collection of electron energy levels at absolute zero. Electrons are dependent on the lattice banding and thus the Fermi level of the Fermi "sea" of electrons present. In the previous section discussing bandgaps, the Fermi level would be set between the valance conduction band at absolute zero (0 K). The equation to describe the energy location is given by equation 21 [14, 21].

$$E_f = \frac{E_{gap}}{2} = \frac{E_c - E_v}{2} \tag{21}$$

This description works well near zero kelvin as the particles obey Boltzmann like behaviors. However, once we begin introducing thermal effects the statistics begin to skew due to energy being introduced into the system thermally. A graph of this is shown below in figure 14.

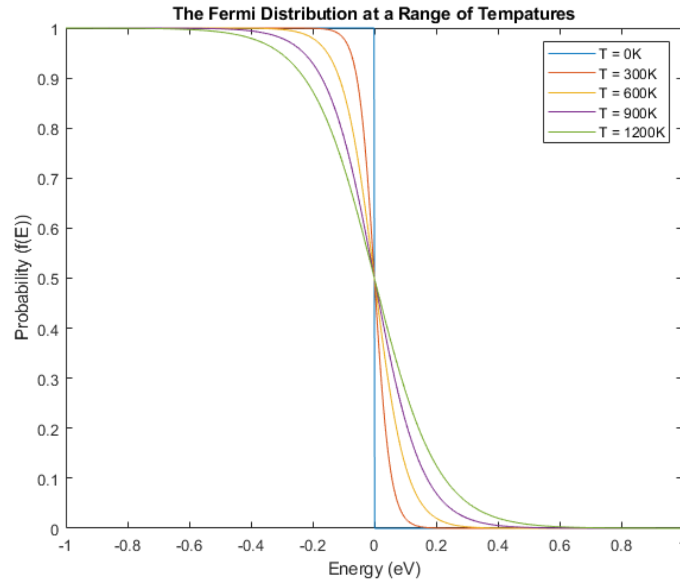

Figure 14: The Fermi distribution at a range of temperatures.

The statistic is also affected by doping and impurities, causing a shift of the Fermi level and thus the Fermi "sea" of elections. This is shown in figure 15 below.

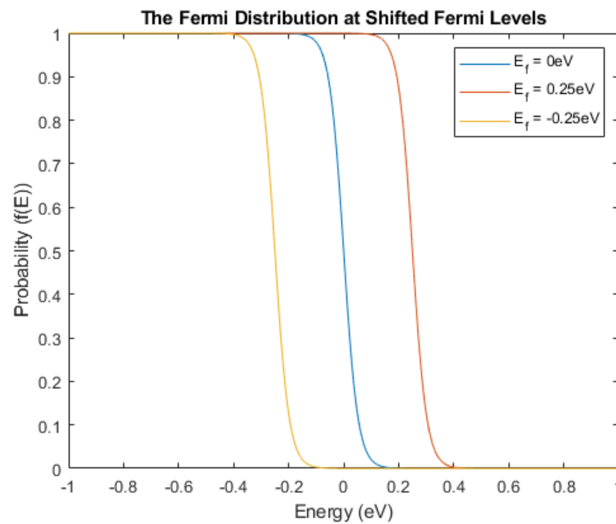

Figure 15: Fermi Distribution at Shifted Fermi Levels

An interpretation of this function is that at ordinary temperatures, most levels up to the fermi level are filled with electrons (thus have a high probability of being found). With higher temperatures, the skew of the function shows that a larger fraction of the electrons can exist above and contribute to conduction band

interactions. It should be noted that even though there are values at the gap between the Fermi level and the conduction band, no electrons exist at the band gap. In the density of states function, it is considered to be the probability that an electron exists at that energy at the given temperature. Due to impurity shifting, this can cause a bit of a recursive relationship to occur due to the Fermi level's dependence on the dopant shift and the amount of dopant that can be calculated to exist to be determined by the shift of the Fermi level.

Dopant and Fermi level shifting

Dopants are purposefully introduced impurities into a semiconductor lattice to make it more conductive and narrow the bandgap between the Fermi level and the conduction band [19, 22]. The prevalence of semiconductors in our modern day is heavily reliant on the relationship between dopant and electrical conductivity. In industry, some of the most common elements for dopant in silicon are boron (B), phosphorus (P), arsenic (As), and antimony (Sb) [22]. The reason behind this is that both elements change the charge carrier distribution of the silicon, allowing for higher conductivity across the lattice due to more availability of charges. Boron has a vacancy in its outer shell allowing for the formation of what is called a "hole." Phosphorus, Arsenic, and Antimony, in contrast, have an extra electron in its valance shell, allowing for more electrons to be introduced into the silicon lattice. The electrons and holes are considered negative and positive charge carriers, respectively. For a visual of this relationship, figure 16 below shows the effects of introduced impurities in the lattice below.

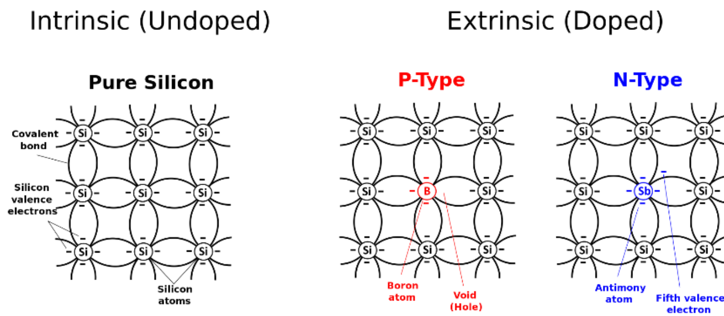

Figure 16: Visual of dopant introduced into the lattice. The right image shows pure silicon without any added dopant while the right image shows two cases: P-Type (Boron doped silicon with extra vacancies "holes" in the lattice) and N-Type (Antimony doped silicon with extra valance electrons). Reproduced from [22].

Introduction of these impurities into the lattice is important as their introduction shifts the Fermi level to allow higher ease of carrier transport as mentioned previously. To introduce these impurities a method known as dopant introduction is used to inject dopant into the semiconductor lattice. By doing this, the newly introduced dopant atom "knocks out" an atom previously occupying lattice point and places itself in that position [22]. After the impurities are introduced through doping the semiconductor, a shift in the Fermi level occurs. This is where more dopant impurities cause the fermi level in the semiconductor to shift up. This relationship is dependent on the dopant introduced into the lattice, however unilaterally the Fermi level will shift up relative to the dopant introduced. There however can be cases where the Fermi level can shift up near the conduction band. This is considered to be when the semiconductor goes to a degenerate state. *Degeneracy* is when the semiconductors' valance band begins to share states with the conduction band due to bandgap narrowing effects. This can cause the semiconductor to exhibit metallic like electrical behaviors [23]. Once the valance and conduction bands begin to fully overlap, this will cause the phenomenon of bandgap narrowing to occur. This leads to the semiconductor exhibiting complete metallic behaviors. An illustration of this phenomenon is shown in figure 17 below.

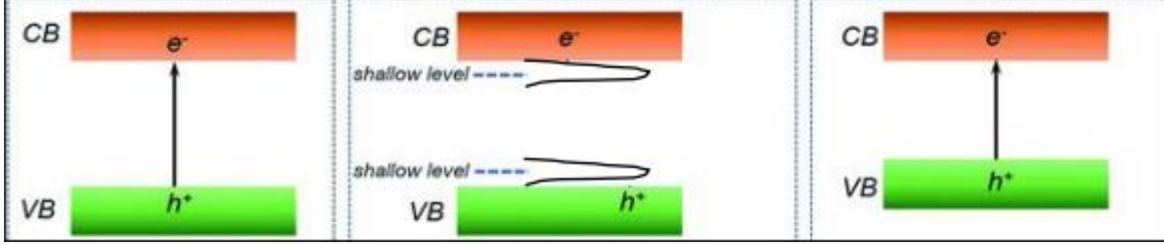

Figure 17: A depiction of band gap narrowing within a semiconductor device. Once enough dopant has been introduced into the lattice of the material, the bandgap will begin to narrow. This leads to more metallic like electrical conductivity within the semiconductor. Reproduced from [24].

To calculate the amount of shifting and degeneracy that occurs due to the Fermi level, the relationship between the dopant amount and the Fermi level can be used. Normally, an equation called the Fermi-Dirac integral is used to determine the relationship between the conduction electrons and shifted Fermi level due to dopant [23,24]. The equation for the Fermi-Dirac integral is shown below in equation 22.

$$F_k(\eta) = \int_0^\infty \frac{x^k}{e^{x-\eta} + 1} dx \tag{22}$$

With k representing the order of the integral and η representing the energy of the electron sea. This equation can often prove to be difficult to solve for as the half-order of this function must be taken without knowledge of η or little knowledge of it. So, approximations are often made in the field of bandgap engineering. An example of these types of approximations is shown below in equations 23 and 24 for the position of the fermi level [24].

$$E_F = E_c + k_b T \left[ln\left(\frac{n_0}{N_c}\right) + 0.353 \frac{n_0}{N_c} \right] \tag{23}$$

$$E_F = E_v - k_b T \left[ln\left(\frac{p_0}{N_v}\right) + 0.353 \frac{p_0}{N_v} \right] \tag{24}$$

Where E_V is the energy position of the valance band, N_v is the effective density of states in the valance band, N_c is the effective density of states in the conduction band, n_0 is the number of electrons, and p_0 is the number of holes. The position and availability of these electrons then can affect many of the thermal characteristics of the semiconductor. Especially when it relates to phonons and three phonon scattering.

Phonons & Three Phonon Scattering

In a lattice of any material, the atoms are in constant vibrational motion as any temperature above absolute zero (0 Kelvin) [25]. Atoms do not move without being acted upon by other atomic forces as their movement is dependent upon their nearest neighbors and the interatomic forces being applied to them. This consequently causes the vibrations and movements of one atom to affect the neighboring atoms and causes a lattice vibrational wave to occur. To make this concept clearer, a toy model can be made using a 1-d chain of atoms, all connected in a row and bonded together one by one as shown below in figure 18 [19].

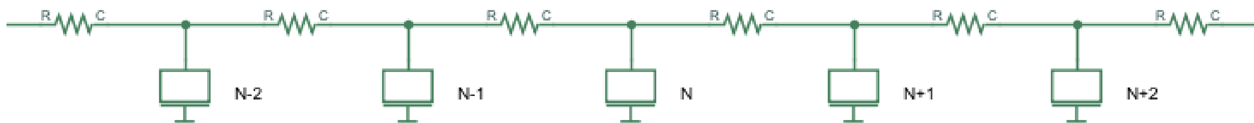

Figure 18: 1-D Toy Model of an Atomic Chain

Where the blocks represent the individual atoms in the lattice and the springs represent the interatomic bonds between each atom. If any of the atoms are displaced from their equilibrium position, this would exert a force on the connecting atoms in the chain both left and right and this force would propagate along the line of atoms. This is an example of a propagating vibrational waves, and in this case the vibration propagates along the one-dimensional chain. The quantum mechanical nature of particles at this scale dictates that the atoms can only vibrate at discrete, quantized energy levels. This can be represented as a simple quantum harmonic oscillator. In a bound potential, which is represented as a parabolic energy curve, the vibrations are discrete levels up the curve. On these energy levels, the wavefunction can be overlayed on each energy level, as that is where the atom exists at that state as shown in figure 19 below.

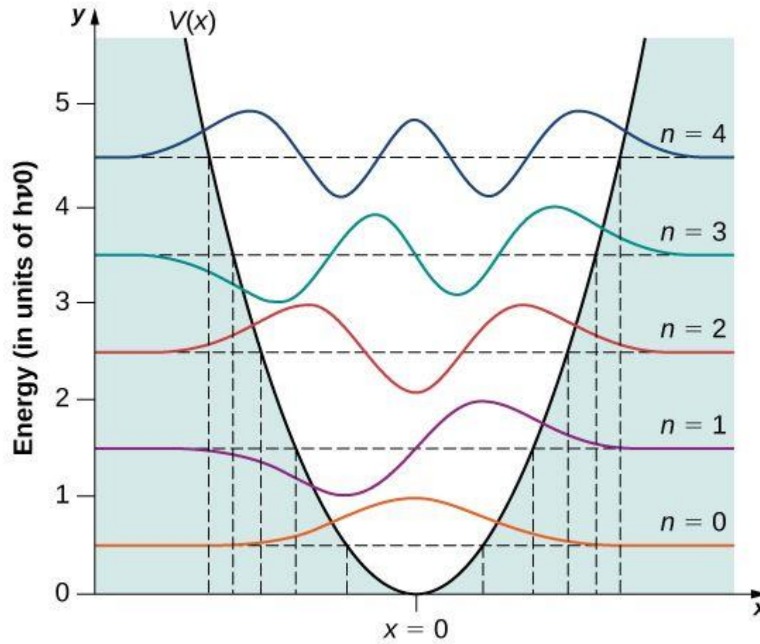

Figure 19: Parabolic Potential Curve and Its Associated Energy Modes with the overlayed wavefunction for each energy level. Sourced from [26].

These normal modes up this energy ladder are considered to be an excitation up the oscillator's potential. This is in essence what a phonon is, a discrete packet of vibrations each with an assigned energy level. This is analogous with the discrete amount of energy transmitted with a photon in the electromagnetic spectrum [27]. The amount of energy in each phonon is related to the frequency of the vibration using the energy frequency relationship. All objects within the nanoscale world exhibit wave/particle duality and are governed by the uncertainty principle. So, phonons can be thought of as pseudo-particles [5]. This description is sufficient if the length scales that are being considered are larger than the wavelength of the phonon. As elementary excitation of the lattice, multiple phonons can exist within the same excitation energy state. This implies that they follow Bose-Einstein statistics and the probability that a phonon is occupying a certain excitation number (the energy level number in our case) [19]. The phonon occupation is directly correlated with how many phonons are occupying in a given volume V of real space. In real lattices, the determination of normal modes available to the phonons amounts to the determination of the dispersion relationship. The dispersion relationship describes the relationship between energy and momentum for

phonons in the lattice of the given material [19]. In solid state physics the dispersion relationship is often shown as a frequency vs. wavevector graph for phonons. Shown below is the dispersion relationship for the one-dimensional lattice shown in figure 20.

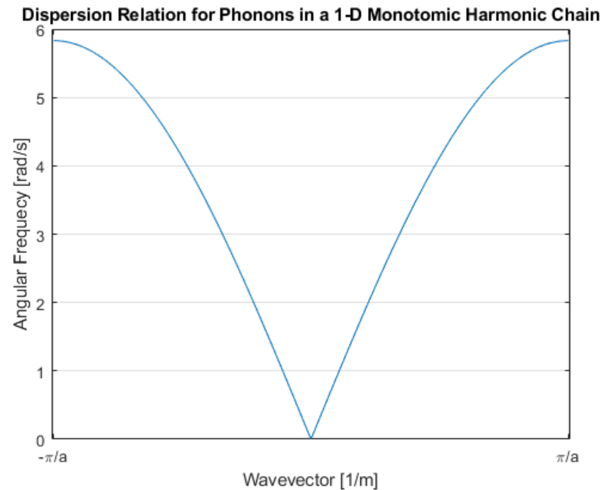

Figure 20: Dispersion Relationship of a 1-D Monatomic Chain, with a representing the lattice spacing between the individual atoms. [19]

This relationship is directly related to the structure of the material and the interatomic forces acting upon each atom. The materials under consideration, silicon, and germanium, have a diamond centered crystal structure. To analyze the structure when relating to dispersion, it is better to look at the lattice in wavevector space (k-space, or sometimes referred to as reciprocal space or the momentum space as mentioned above). Wavevector space is formed by taking the three-dimensional spatial Fourier transformation of the real lattice space. For analysis, we consider a zone called the First Brillouin Zone (FBZ). The FBZ represents the basic unit cell in wave vector space and the physically possible values of the wavevectors for each phonon [5,19]. Wavevectors that reach beyond this space can be related back to the FBZ through the concept of aliasing, where the wavevector is mirrored back to the FBZ due to having similar locations and values of another wave in a different cell of the lattice [28]. The edge of the FBZ represents the minimum meaningful wavelength relative to the lattice. A schematic of the FBZ for silicon is shown below in Figure 9.

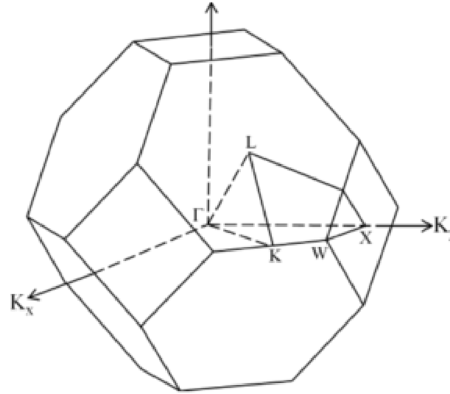

Figure 21: First Brillouin Zone of Silicon, Reproduced from [5].

Each axis labels the different components of the allowable wavevectors. In solid state physics, certain locations are labeled with the letters Γ, L, X, K, and W shown in Figure 21. The labels are used to denote the directions of high symmetries within the lattice itself [14,19]. For example, the direction of Γ-L is referred to as the (100) vector of the lattice and denotes the direction of propagation of the phonons in a direction parallel to one edge of the cubic unit cell as shown in Figure 1.

Six energy levels are available to any one wavevector within the domain of the FBZ for a two-atom basis, like silicon [19]. The energy levels are labeled with different frequencies and are referred to as modes or polarizations. The different modes of each related to the displacement of the adjacent atoms in the lattice c relative to one another. The acoustic modes involve adjacent atoms in the lattice moving in the same direction while optical modes are moving opposite to each other as shown in Figure 22.

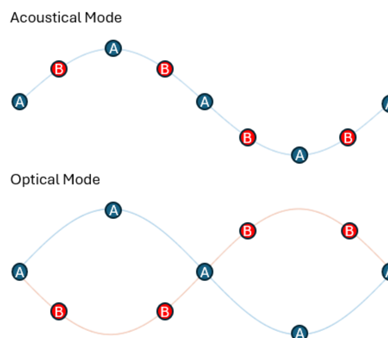

Figure 22: Image of Acoustical and Optical Modes

Within acoustic and optical modes, transverse and longitudinal modes of these waves can be identified. Transverse indicates that atomic motions are orthogonal to the direction of motion of the wave whereas longitudinal is when atomic motions are parallel to the direction of motion of the wave (often called a compression wave). Two transverse directions exist for any given longitudinal direction, and they are also orthogonal to the longitudinal direction. An example of the experimentally determined relationships for this behavior in a silicon lattice is visualized in Figure 23 on a frequency-wavevector diagram.

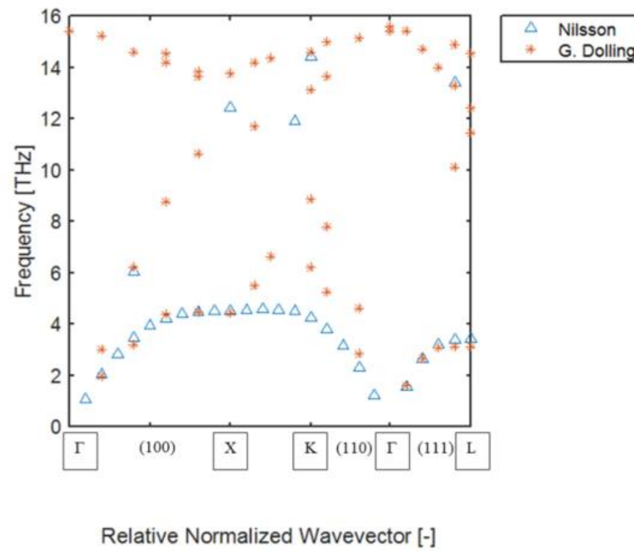

Figure 23: Experimental Values for Silicon Dispersion in the (100) Direction at 300 K. Triangles Are Data from Nilsson and Nelin [29], Open Circles Are from Dolling [30].

Results are shown for frequency vs. wavevector in different directions of the FBZ. The labeling of the graph corresponds to different wavevector lattice points identified in the FBZ labeled in figure 21. Phonons traversing in different directions through the lattice can have different frequencies. This is a result of the different interatomic forces that result in different trajectories in the lattice [25]. As a result, different phonon modes will exhibit different group velocities as they traverse through the material lattice. The group velocity is defined in equation 25.

$$\overrightarrow{v_g} = \frac{d\vec{\omega}}{dk} \tag{25}$$

Graphically, this is interpreted as the slope at any given point on the dispersion curves.

Scattering interactions affect phonon transport just as photon interactions with a refractive crystal affect radiative transport [19]. Phonons can interact with boundaries, interfaces, impurities, transport electrons, photons, and other phonons as well. In pure insulating three-dimensional bulk material, the primary interaction that affects phonon transport is three phonon scattering [19]. Three phonon scattering involves three phonons that can take two forms, type I, and type II. Type I is shown in Fig 24.

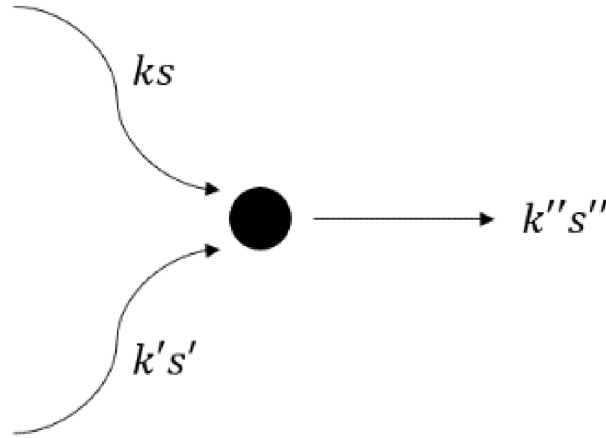

Figure 24: Illustration of 1-D three phonon scattering where ks' and k's' combine to produce k"s", Type II reverse the order. Adapted from [5]

Where k, k', and k'' indicate the wavevectors of the three phonons and s, s' and s'' are the polarizations or modes. In both types of interactions, energy, and momentum (up to a subtraction of a reciprocal lattice vector) is conserved This implies the following relationships regarding the wavevectors and frequencies:

$$ks + k's' = \mathrm{k''s''} + \mathrm{G} \tag{26}$$

$$\omega(\mathrm{k}) + \omega'(\mathrm{k'}) = \omega''(\mathrm{k''}) \tag{27}$$

The only meaningful wavevectors are those in the FBZ. If an interaction involves the addition of wavevectors that lead to a result inside the FBZ it is referred to as a normal scattering event [19]. If an

interaction involves the addition of wavevectors that lead to a result in the FBZ as it is referred to as a normal scattering event. If an interaction involves the addition of wavevectors that results in a result outside of the FBZ domain, it is aliased back into the FBZ. This type of backscattering interaction is known as an Umklapp process. Both types of interactions are schematically shown with figure 25.

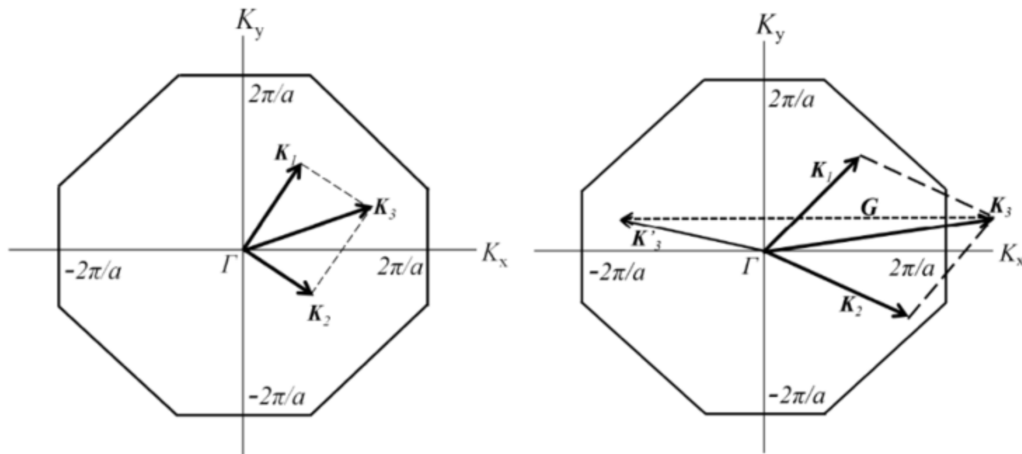

Figure 25: Normal vs. Umklapp three phonon scattering in a 2-d representation of the wavevector space. Phonons K1 and K2 interact to result in vector K3 in the normal process on the left. Phonons K1 and K2 interact to result in K3 that is reflected back into the FBZ with the reciprocal vector G in the Umklapp process on the right. Reproduced from [5].

However, phonons can propagate through other mechanisms as mentioned above. As we add more dopant into the system, the interatomic force constants will change depending on the size of the dopant atom and charge carrier. This. can lead to a production of a perturbation which will lead to a change of state for the phonon [25]. The impurity scattering rates are directly dependent on the square of the frequency of the phonon involved in the interaction, the number of phonons with that particular frequency, and the impurity scattering parameter [5]. This is all a result of dopant concentration and as such an increase in interaction events and thus a general increase of dispersion across the medium. To calculate the number of new interactions due to dopant concentration requires an understanding of fermi effects when dopant concentration is introduced.

Electron and Phonon Interaction Scattering and Heat Generation

As phonons are the main thermal energy carrier in the lattice and thus the semiconductor device, it is the interaction between the phonon and electron populations which give rise to joule heating. Electrons and phonons experience many interactions and transformations as they move through a material lattice. However, electron-phonon scattering is the only interaction that changes the net energy of the electron population as it results in net energy transfer to the lattice structure [5]. The input of energy to the phonon population is primarily due to the deformation potential interaction. With the deformation potential interaction, phonons are assumed to produce a uniform local strain of the lattice structure. This local strain causes a deformation of the electron cloud, influencing charge carrier transport. This is treated as a perturbation responsible for scattering and scattering rates can be computed from Fermi's Golden Rule. Fermi's Golden Rule is shown below [16].

$$\tau = \frac{2\pi}{\hbar}\left|\langle \Psi_f | \widehat{H_{\iota f}} | \Psi_i \rangle\right|^2 \delta(E_f - E_i \pm \hbar\omega) \tag{28}$$

Where τ is the transitional probability per unit of time, Ψ_i is the initial state of the quantum system, Ψ_f is the final state of the quantum system, $\widehat{H_{\iota f}}$ the Hamiltonian dynamical matrix of the system, and $\delta(E_f - E_i \pm \hbar\omega)$ is the energy conservation condition. In the inelastic interaction, the electron will emit a phonon as it transitions to a lower energy state, or it can absorb a phonon to reach a higher energy state. This interaction is shown schematically in the Feynman diagram in figure 26 below.

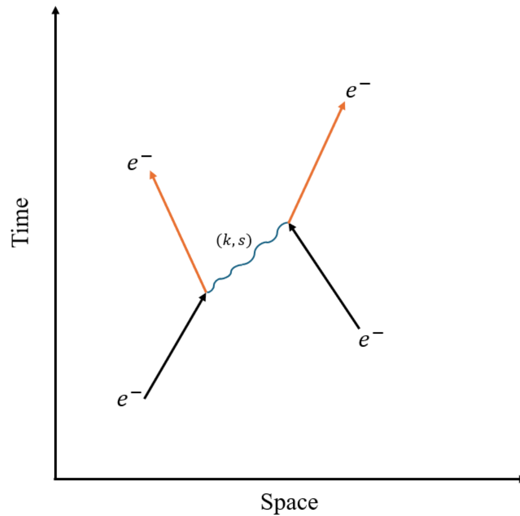

Figure 26: Electron-phonon interaction Feynman diagram. The e^- represent the electrons and the arrows represent the states with the black arrows are the initial states and the orange arrows represent the final states. The wave (k, s) represents the phonon interaction of emission and absorption form one electron to its local neighbor.

In the case where a phonon is emitted and absorbed, the initial state consists of an energy E and a momentum q, the final state with an energy E' and momentum q', and a phonon with momentum k and polarization s.

Modeling Implementation

Methodology

Implementation of Fermi's Golden Rule for electron-phonon scattering requires the knowledge of the interactions allowed by the selection rules, the deformed potential, and the initial phonon and electron populations. The electron population initialization within the conduction band is the focus of this work and for a visual of this, figure 27 below shows the block diagram representing the steps and how they feed into each other sequentially.

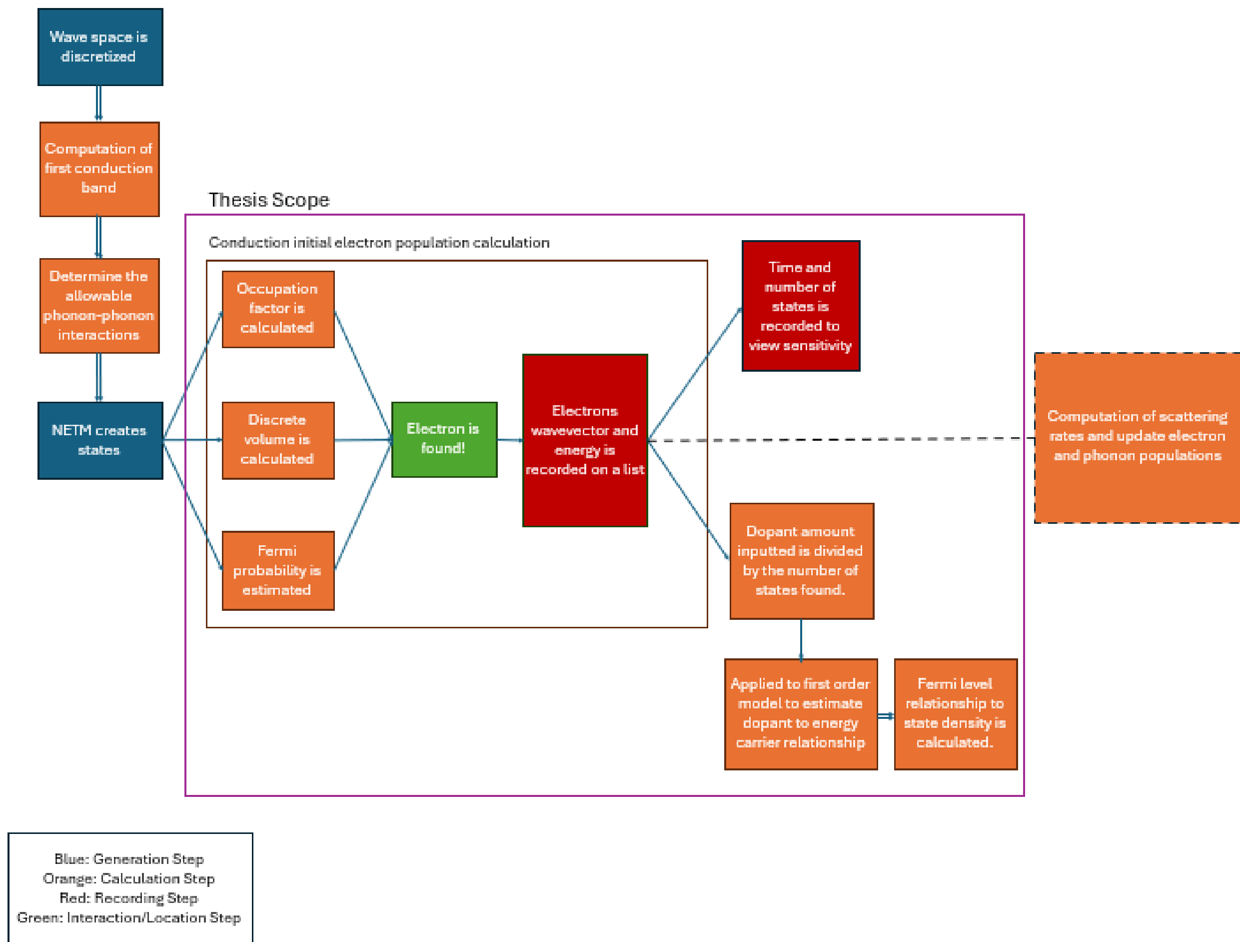

Figure 27: Visual guide for modeling approach and steps. Solid lines represent work done; dashed lines represent future work to be done.

Electron Population

To compute the distribution of electrons at or above the conduction band minimum, the relationship for both the density of states and probability function needs to be found for each wavevector space element. A depiction of this method is shown below in figure 28.

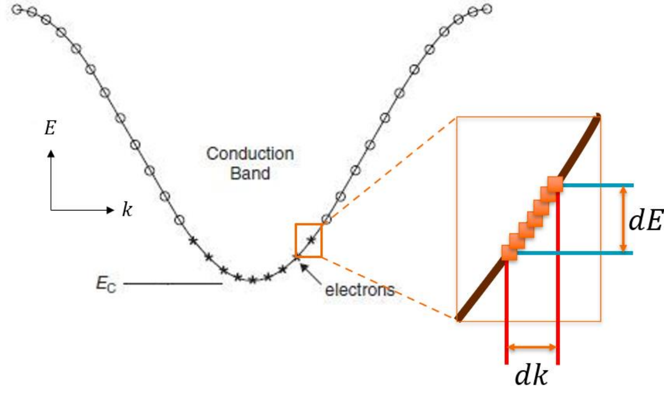

Figure 28: A depiction of the states located along the conduction band. Each state at the conduction band will exist among a dk interval in dE energy range. As such, a relationship between dk and dE can be used to find all the states located along the interval.

To model this for the NETM, the given volume in real space is given by the following equation:

$$\mathrm{dV} = \mathrm{dx} * \mathrm{dy} * \mathrm{dz} \tag{29}$$

This in it of itself is simple to explain, where dx, dy, and dz are the discretized lengths in real space which is computed by the NETM in the input scattering algorithm. To obtain the occupation factor, there will be a set amount of occupancy per unit of k space. This can be represented by the following relationship:

$$occupancy \propto dk \tag{30}$$

Remembering that in order to translate that occupancy per dk into real space requires use of the inverse Fourier transform, the following relationship is then made for all of the conduction band.

$$occupancy\ factor = \frac{dk^3}{(2\pi)^3} \tag{31}$$

After this, the probability of finding an electron in real space is then simply the Fermi-Dirac distribution. Multiplying all of these together, a relationship is given by the following equation:

$$N(E)dE = (dx * dy * dz)\frac{dk^3}{(2\pi)^3}\frac{1}{1 + e^{-\frac{E(k)-E_f}{k_b T}}}dE \tag{32}$$

Finally, to find all the possible electron elements that are applicable for the initial state calculations, a sum over all k-space is done using the energy-wavevector relation. For a continuous distribution this would be done with an integral, but computationally this is done as a sum. This is shown in equations (33) to (35).

$$N(E)\,\hbar dk = (dx * dy * dz)\frac{dk^3}{(2\pi)^3}\frac{1}{1+e^{-\frac{E(k)-E_f}{k_b T}}}\,\hbar dk \tag{33}$$

$$e_{\#}^{-} = \int (dx * dy * dz)\frac{dk^3}{(2\pi)^3}\frac{1}{1+e^{-\frac{E(k)-E_f}{k_b T}}}\,dk \tag{34}$$

$$e_{\#}^{-} = \sum_{k} (dx * dy * dz)\frac{dk^3}{(2\pi)^3}\frac{1}{1+e^{-\frac{E(k)-E_f}{k_b T}}} \tag{35}$$

It should be noted that the same equation can be used to find any matter of electrons across the entire band energy spectrum. However, conduction electrons are only considered as they are the only contributors to the charge carrier movement and thus the electron-phonon interactions.

Dopant Charge Carrier Contribution Population Initial Implementation

When it comes to dopant modeling, given all the considerations given in the literature it was difficult to create a "shoe fits all" model for the current stage of the NETM. This would require code for every element used and an implementation of Fermi-Dirac integration. For a simple model however, it was considered that all dopants were ionized and filled spots in the silicon conduction band. Thus, every electron effective state found would be proportional to the amount of total distribution of the dopant across the lattice. This can be represented with the following mathematical relationship:

$$e_{\#}^{-} * \alpha = dopant\ charge\ contributions \tag{36}$$

As such, to find that proportionality, a simple mathematical relationship can then be used:

$$\alpha = \frac{Dopant\ Input}{e_{\#}^{-}} \tag{37}$$

Of note is that this calculation could work for any type of dopant as long as the charge carrier addition is one to one. That is, for every ion added either there must be one additional electron or additional hole. This represents the Fermi-Dirac integration of finding the dopant relation to the number of effective states and as such can be used as a replacement. As such, to compute a new fermi level, the constant α can be used in conjunction with equation (25) to produce the following Fermi shift model:

$$E_f = -k_b \mathrm{T}\left[ln\left(\frac{1}{\alpha}\right) + 0.353 * \frac{1}{\alpha}\right] \tag{38}$$

There is no conduction band addition as the model considers the conduction band to be the initial band edge value.

Electron Phonon Mesh Analysis

The wavevector element size was investigated to determine the effect on allowable electron-phonon interactions subject to the conservation of energy and momentum. The mesh sensitivity consisted of variation of element sizes to three values and resulting search of the wavevector space. The allowable interactions were recorded and added to the collective bin. For the mesh sizes ran, the range was determined to be between mesh size ten and mesh size twenty as to see how the splitting of wavevector space would cause the bin sizes of wavevector and energy space to change over the size gradient. Of the interactions that were run, the final time to compute was recorded and was checked to see how the results would relate to the number of interactions found in the lattice. Then a histogram chart was made to view the group trend and understand more the importance of mesh size to interactions found in the lattice.

Validation and Modeling Results

Comparisons to Published Literature

Rowlette and Goodson Simulations

Goodson, Pop, Sinha, and Rowlette have already done much in the area of thermal and electrical modeling in nanoscale Field Effect Transistors (FET's). The work chosen for comparison of the density of states model is that of Rowlette and Goodson [13]. With this work, a one-dimensional simulation of silicon PNP (positive negative positive) junction transistors were used to represent the core of the transistor structure. The device consists of a 150nm source (S or n+), and drain (D or n+) separated by the gate channel (Channel, or p) of 20 nanometers. The channel is below the gate region between the gate and interface. Schematically these are shown below and illustrated with figure 29.

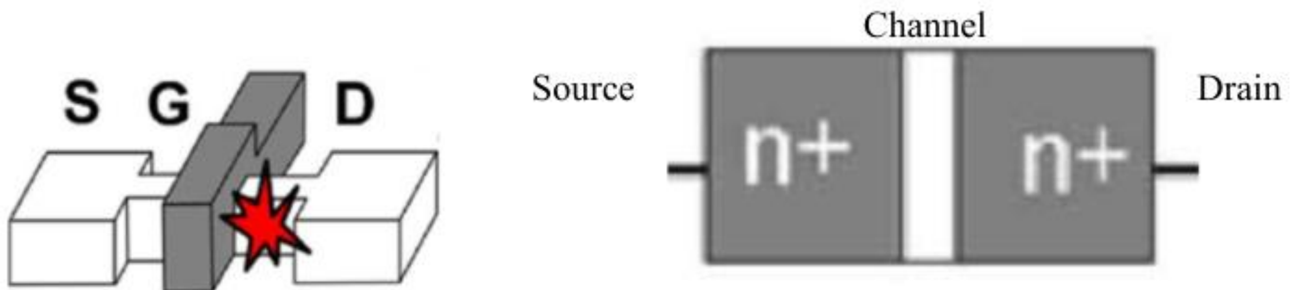

Figure 29: Schematic illustration of the one -dimensional domain simulated by Rowlette and Goodson [13].

For density of state calculations, the banding was approximated using a parabolic model at the (100) lattice face. This utilized an effective mass factor and an empirically derived tight chain binding model as derived from T. B. Boykin et al [31]. This approximation allowed for most of the valance band charge carrier transport to occur at the (100) direction and fit accurately to the empirically gathered data set. This was used as a starting point to test if general DOS calculations were fitting with empirically measured methods.

Jin and Fischetti

Jin, Fischetti, and Tang [32] performed electron mobility modeling on a silicon wire to set for surface roughness effects and band non-parabolicity. In this work they utilized the Kubo-Greenwood formula for material electrical conductivity in tandem with the self-consistent solutions to both Schrodinger's equations and Poisson's equations for elliptical surfaces. This was applied to a silicon wire with a variable diameter, a diagram of which is shown in figure 30.

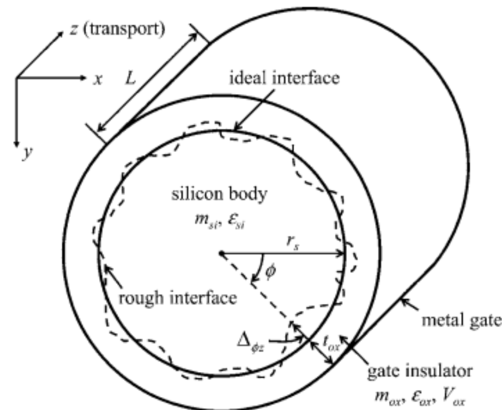

Figure 30: Schematic of a gated nanowire structure that was considered under the Jin and Fischetti Study [31]

The diameter considered for testing was 3nm diameter, as now with current transistor nanowires a 3nm process is used to allow confinement in the x and y direction while streamlining the charge carrier transport. For the testing of the density of states, their output of the 3nm density of states was used due to 3nm being a standard feature size for the more modern transistors in current day computational devices.

Martin and Gonzalez: One Dimensional Electron Transport Analysis

Martin, Gonzalez, Pardo, and Velazquez [33] utilized a one-dimensional Poisson solver with a Monte Carlo simulation to solve electron transport in homogeneous Si structures in PNP diodes. For their simulation, they first simulated under the conditions of bulk silicon and then under homogenous diode structures. For the bulk silicon, a 1-D study was conducted to see how the model faired under bulk 1-D confined silicon. A visual of this is shown below in figure 31.

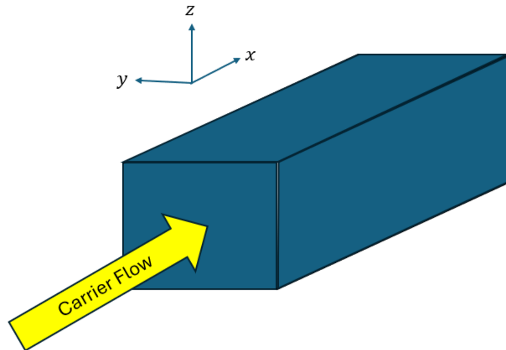

Figure 31: Bulk Silicon wire model used in Martin and Gonzalez [32].

Second, they utilized their model in a comparison of PNP junction transistors in the field directions of $< 100 >$ and $< 111 >$ lattice directions. This was done to test the model for charge carrier transport in different device configurations. As they utilized a one-dimensional model, direct comparison can be made to the NETM's silicon nanowire FET capabilities. The density of states model that they used involved a two-valley model in the lattice direction. The model came exceedingly close to real predictions and fitted well to the conduction band curvature in the $< 100 >$ direction. As such, their density of states model will be used as well to compare between electron locations.

Ashraf: Intrinsic Carrier Concentration in Presence of Degenerate Doping

Ashraf pointed to inaccuracies in previous literature relating to bandgap narrowing parameters [34]. Utilizing analytical equations, he pointed out that much of the literature previously failed to account for bandgap narrowing parameterizations and suggested a doping dependent model at 300K. His results for the Fermi Energy will be used as analysis in this paper to measure the new algorithms capabilities of accurately predicting band gap narrowing within semiconductor devices and to point towards any improvements needed to the bandgap model currently used.

Results Discussions

Density of States

For density of states, a comparison was made to the model done by Jin et al [32]. Their calculations included the entire range from the valance to the conduction band, but only the conduction band results were considered due to the nature of electron-phonon interactions. The results for the density of states occupation factor distribution are shown in figure 32.

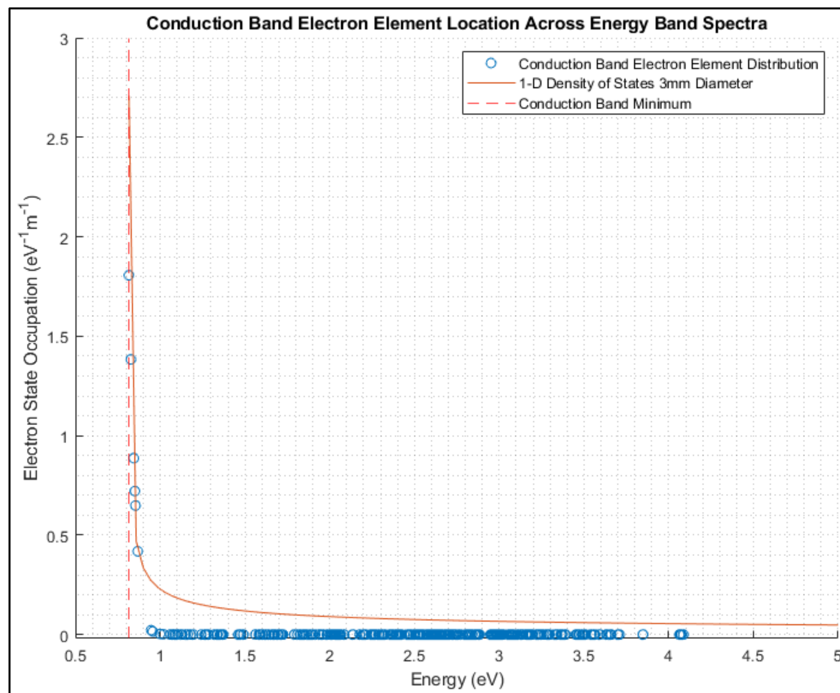

Figure 32: Dopant Electron Element Occupation Locations across the energy spectra. The results for the 3mm diameter wire from Jin et al [31] are shown as the red line.

There is much agreement with the results collected in comparison to Jin's model. In the worst case, it appears that due to the electrons rapidly falling into the bands below, they no longer agree. As we are only looking at conduction electrons, it makes sense to say that the convergence would go near zero and Jin's model does converge into a near zero probability at the band edge. For E-k diagram results, figure 33 shows these results as well.

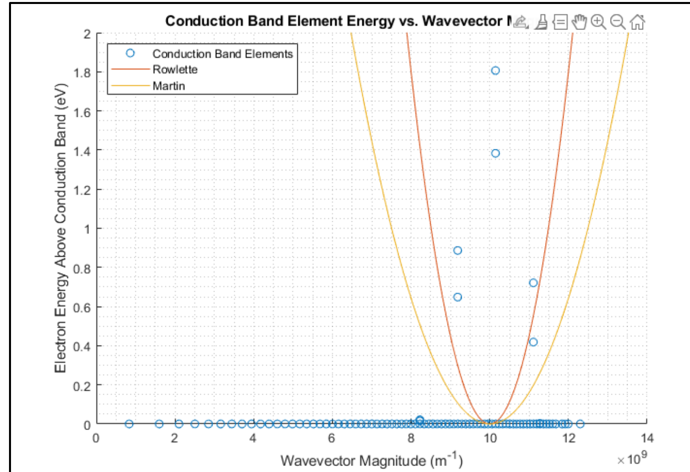

Figure 33: E-K Diagram results for the new model, with the NETM results represented in the blue circles, Rowlett et al [13] is represented in red, and Martin et al [32] is represented in yellow.

There is much agreement with the distribution of states among the two models as the wavevector magnitude of $10 * 10^9 m^{-1}$ represents the X direction of the FBZ.

Dopant Correlation Results

For dopant there were some observations done on the relationship between states and dopant, most involving the position of the fermi level and the dopant parameter. Figure 34 shows the relationship between the proportionality constant and amount of dopant.

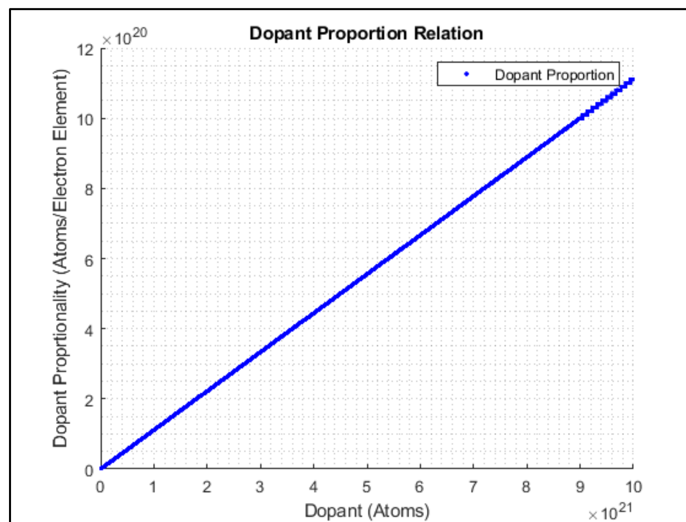

Figure 34: Dopant relationship to dopant proportionality.

The model is mostly linear in the resultant curve. However, it should be noted that at the end of the curve a jaggedness in the line begins to appear. This could be due to the effect of degeneracy and stacking of states at higher dopant amounts. For the Fermi level shift, a computation was performed afterwards to observe the shift in level and the dopant proportionality correlation to the data collected by Ashraf. Below in figure 35 is a model of the data correlation:

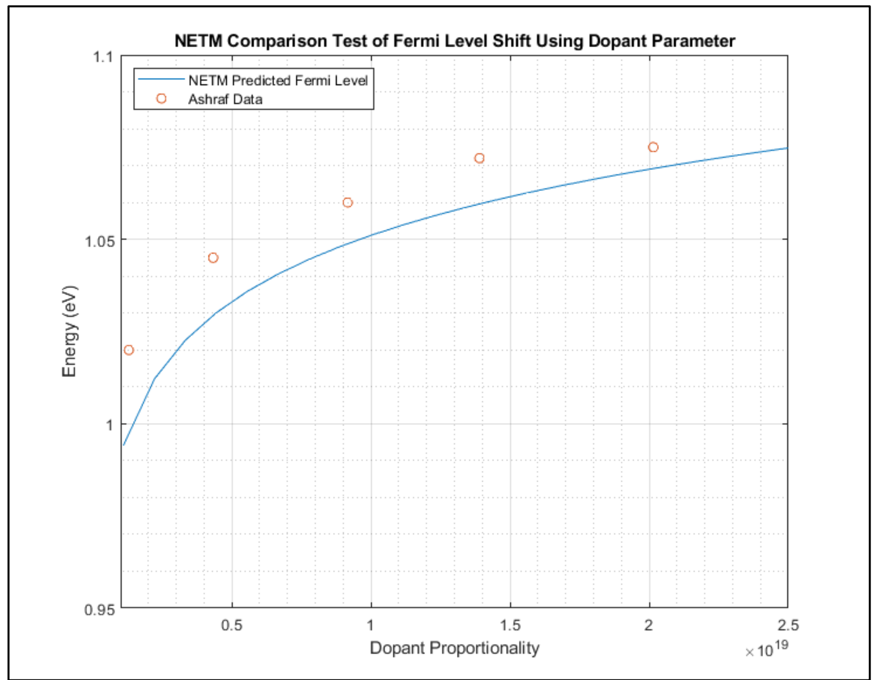

Figure 35: NETM Algorithm comparison with Ashraf [34]. The blue line represents the NETM algorithm predictions while the red circles represent data from Ashraf.

As shown, the NETM produces a reasonable fit to the predictions from Ashraf [34]. There is however a slight lowering of the curve in comparison. This could be a result of the handling of the conduction band calculations in the NETM, as the set value (0.81517 eV) is lower compared to the experimental value recorded in the literature (1.12 eV).

Mesh Sensitivity Results

For the mesh sensitivity, twenty runs of the NETM were done in order to collect the aggregate results across all meshing conditions. This went from a range of ten to twenty in terms of mesh slicing and this was done

all on the same machine to reduce variability in results. The following two graphs (Figures 36 and 37) were produced afterwards as a measure of the results.

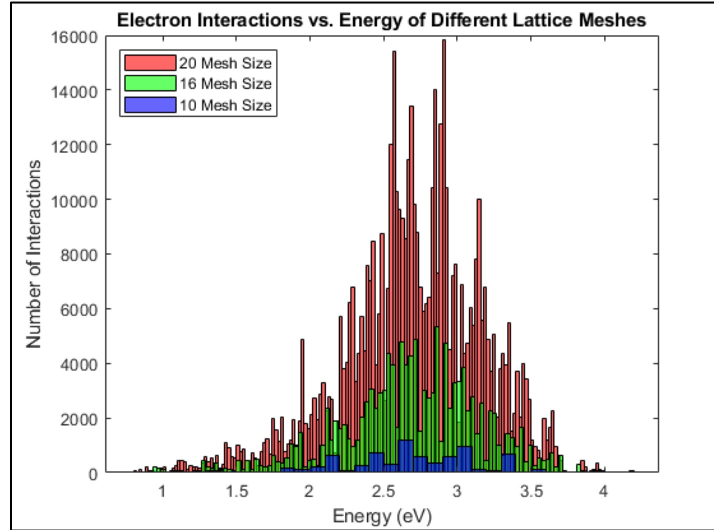

Figure 36: Mesh Sensitivity Test Histogram Relating Energy Values vs Interaction Count.

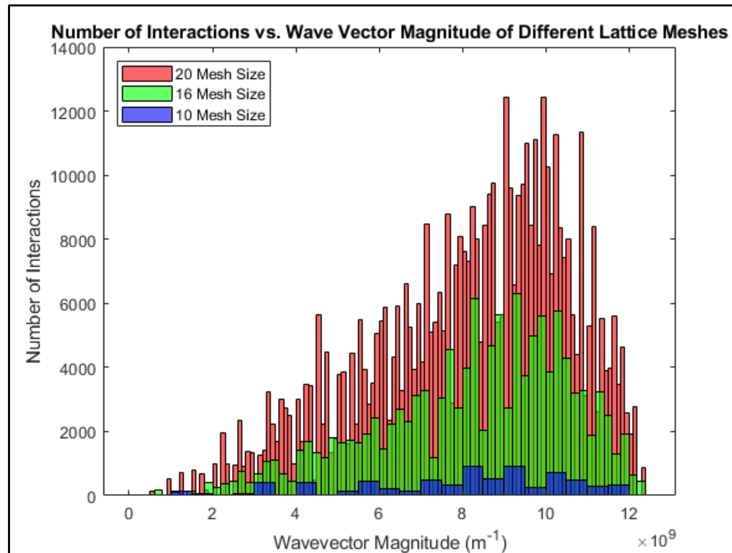

Figure 37: Mesh Sensitivity Test Histogram Relating Energy Values vs Interaction Count.

As a general observation, the finer the mesh size came with finer results and more interactions seen. This means that the more we partition the FBZ mesh, the more interactions are generated and analyzed. This is seen in both the energy and wavevector results. The significance of this in the wavevector domain is that it

corresponds well for the electron locations across the conduction band seen above at the previous section and the optical phonons peak as related to NETM three phonon scattering output at the X FBZ direction [5]. This also remains consistent with the lower edge conduction band edges shown in both Rowlette [13] and Martin [33]. This means that it is expected that at that orientation there should be more interaction between the electrons and phonons that can only be seen in 12+ mesh sizing. This could have a significant impact on FGR implementation in the future and should be considered for future implementations.

It should be noted that even though there are more interactions seen, this increases computation time significantly. For a peak mesh size of twenty, the number of interactions calculated made the runtime peak for the NETM was 3 hours total given the finer interaction and meshing in comparison to the regular run time of 30 minutes for sub-sixteen meshes. So, the finer the mesh, the more time will be taken to run all interaction iterations.

Summary, Conclusions, and Future Work Recommendations

Summary

The work presented accomplished the original three goals for the new additions of the Nanoscale Energy Transport Model:

1. Initialize the electron population within the conduction band allowing for consideration of both doped and intrinsic charge carriers.

2. Understand the proportionality of dopant vs. the number of electrons present above the conduction band by using a first order model.

3. Look at the mesh sensitivity of the wavevector space element size to the electron-phonon interaction statistics and look into the number of interactions related to those statistics.

These were all addressed with new additions to the existing Nanoscale Energy Transport Model and a measurement of its accuracy to existing work. The major addition now added is computation of states that are initialized at the conduction band including scanning for the individual energies and wavevector magnitudes of each charge carrier.

First, utilizing density of states theory, a new model was developed to allow computation across the entirety of the conduction band for both doped and intrinsic electron states. This computational utility allows for electron look up and initial state initialization for Fermi's golden rule functionality. Second, a preliminary dopant scaling model was added to allow scaling factors for how much dopant the user wishes to input into the lattice of dopant in comparison to the number of states found. Finally, a mesh sensitivity test was done to see how these additions affected the model interactions and interaction counts and run time. The density of state model was tested against other representative simulations from literature and showed accuracy among its contemporaries.

Conclusions

From the NETM, it can be concluded that electrons are less likely to exist higher up the conduction band limits, much like observed phenomena. Along with this, the dopant relationship with these found electrons is linear until the amount of dopant starts to cause band gap narrowing in the device structure. For meshing, smaller mesh sizes lose accuracy but can be speedily done. However, for an accurate simulation, large mesh sizes are preferable. And now the NETM has implemented initial state functionality. Thus, the NETM is now ready for Ferm's golden rule implementation.

Future Work Recommendations

The work presented now in this dissertation illustrates some more enhancements to the NETM; however, a number of additional extensions should be considered for future work. As the comparison of the NETM to

other modeling techniques form the literature has illuminated more issues with the NETM and its modeling of joule heating. This can be represented as the following research question:

Can the Nanoscale Energy Transport Model be able to provide high fidelity, transient, 3D simulations of nanoscale devices with full charge carrier and phonon transport and predict the effect the design parameters of volage biases, dopant, topology, and heat transfer to effect device performance, maximum clock speed, and thermal failure limits?

Any extensions beyond this point should be focused on answering the above question. For some proposed future work, some avenues that could be taken are:

1. Fidelity
    a. Fermi's Golden Rule Implementation for electron phonon interactions
        i. As Fermi's golden rule allows for calculation of joule heating in the interactions between phonons and electrons, this should be considered a high priority for implementation. With the additions added in this dissertation, there now should be a basis to allow full FGR implementation for electron-phonon interactions.
    b. Impurity scattering
        i. Nanoscale devices primarily consist of dopant as mentioned above to increase conductivity. The addition of states that include impurity scattering proportional parameters should be included for higher fidelity dynamics. This could also include a distribution algorithm as well for impurities based on the semiconductor manufacturing process.
    c. Silicon Oxide Support

i. Due to the use of silicon oxide in semiconductor manufacturing, a next-generation model should include phonon transmission between silicon and silicon oxide material regions to accurately capture heat transfer across the device boundary.

2. Flexibility
    a. Curvilinear coordinates or topological principles could be implemented to provide wider support for discontinuities in the lattice topology.
    b. Change of basis and tensor implementation will allow for better general representation of non-cartesian topologies in lattice or transistor structures.
    c. Multi-scale and Levi-Civita connection implementation could allow the merger of local transport model with disjointed and larger scale coordinate system modeling where Fourier's law can be used.
3. Computational Efficiency
    a. Implementation of the CUDA® toolkit from NVIDIA® will allow hardware acceleration to be an option for the NETM. Greatly increasing performance across the board with the use of Tensor Core implementations.

These improvements of the NETM made in this dissertation and suggested with the future work will contribute to enhancing nanoscale device designs and a better understanding of local thermodynamic conditions. It is the sincerest hope of the author of this thesis that the development of this model will lead to an improvement in engineering considerations and design decisions for nanoscale devices and, ultimately, lead to the betterment of society. Whether it be in a big or small way.

References

1. Will Fox. (2020). *Computers & the Internet*. FutureTimeline.

2. *Transistor Count Trends Continue to Track with Moore's Law*. (2020, March 5). Design and Reuse.

3. Karl Rupp. (2022, February 22). *Data Repository for My Blog Series on Microprocessor Trend Data*. Microprocessor Trend Data.

4. Wim Slagter. (2020, October 29). *Hardware Tips to Accelerate Simulation*. ANSYS Blog.

5. Medlar, M. P., & Hensel, E. C. (2022). An Enhanced Statistical Phonon Transport Model for Nanoscale Thermal Transport. *Journal of Heat Transfer*, *144*(8). https://doi.org/10.1115/1.4054600

6. H. S. Carslaw, & J. C. Jaeger. (1986). *Conduction of Heat in Solids* (2nd ed.). Oxford University Press.

7. Robert W. Fox, Alan T. McDonald, & John W. Mitchell. (2020). *Introduction to Fluid Mechanics* (10th ed.). Wiley.

8. Chang, C. W., Okawa, D., Garcia, H., Majumdar, A., & Zettl, A. (2008). Breakdown of Fourier's Law in Nanotube Thermal Conductors. *Physical Review Letters*, *101*(7), 075903. https://doi.org/10.1103/PhysRevLett.101.075903

9. Yang, N., Zhang, G., & Li, B. (2010). Violation of Fourier's law and anomalous heat diffusion in silicon nanowires. *Nano Today*, *5*(2), 85–90. https://doi.org/10.1016/j.nantod.2010.02.002

10. Chen, G. (2005). *Nanoscale energy transport and conversion: a parallel treatment of electrons, molecules, phonons, and photons*. Oxford University Press.

11. Shindé, S. L., & Srivastava, G. P. (Eds.). (2014). *Length-Scale Dependent Phonon Interactions* (Vol. 128). Springer New York. https://doi.org/10.1007/978-1-4614-8651-0

12. *14th Gen Intel® Core™ Desktop Processors*. (2024). Intel.

13. Rowlette, J. A., & Goodson, K. E. (2008). Fully Coupled Nonequilibrium Electron–Phonon Transport in Nanometer-Scale Silicon FETs. *IEEE Transactions on Electron Devices*, *55*(1), 220–232. https://doi.org/10.1109/TED.2007.911043

14. Kurinec, S. K. (2023). *Quantum and Nanostructures Fundamentals*. Rochester Institute of Technology.

15. *Silicon Crystal Structure*. (2024). Hyperphysics. http://hyperphysics.phy-astr.gsu.edu/hbase/Solids/sili2.html

16. David Jeffrey Griffiths, & Darrell F. Schroeter. (2020). *Introduction to Quantum Mechanics* (11th ed.). Cambridge University Press.

17. Michael Dayah. (2022, October 12). *Periodic Table*. https://ptable.com/?lang=en#Properties

18. Richard Phillips Feynman, Robert B. Leighton, & Matthew Linzee Sands. (2011). *The Feynman Lectures on Physics* (4th ed., Vol. 3). Basic Books, a member of the Perseus Books Group.

19. Steven H. Simon. (2013). *The Oxford Solid State Basics*. Oxford University Press.

20. Verhulst, A. S. (2004). *Optical pumping experiments to increase the polarization in nuclear-spin based quantum computers*.

21. Sethna, J. P. (2023). *Entropy, Order Parameters, and Complexity*.

22. Kurinec, S. K. (2023). *Semiconductor Process Engineering: Overview & Microelectronics Fabrication Principles*. Rochester Institute of Technology.

23. Lanyon, H. P. D., & Tuft, R. A. (1979). Bandgap narrowing in moderately to heavily doped silicon. *IEEE Transactions on Electron Devices*, *26*(7), 1014–1018. https://doi.org/10.1109/T-

ED.1979.19538

24. Kurinec, S. K. (2021). *Degenerate Semiconductors and Band Gap Narrowing*.

25. John Michael Ziman. (1962). *Electron and Phonons*. Clarendon Press.

26. Geesink, H. (J H., & Meijer, D. K. F. (2019). A novel biophysical quantum algorithm predicts super-conductive properties in animate and inanimate systems. *Quantum Biosystems*, *10*(1), 1–32.

27. Chen, G. (2005). *Nanoscale energy transport and conversion : a parallel treatment of electrons, molecules, phonons, and photons*. Oxford University Press.

28. Thomas III Brown. (2012). *A Statistical phonon transport model for thermal transport in crystalline materials from the diffuse to ballistic regime*.

29. Nelin, G., & Nilsson, G. (1972). Phonon Density of States in Germanium at 80 K Measured by Neutron Spectrometry. *Physical Review B*, *5*(8), 3151–3160. https://doi.org/10.1103/PhysRevB.5.3151

30. Dolling, G., & Cowley, R. A. (1966). The thermodynamic and optical properties of germanium, silicon, diamond, and gallium arsenide. *Proceedings of the Physical Society*, *88*(2), 463–494. https://doi.org/10.1088/0370-1328/88/2/318

31. Jin, S., Fischetti, M. v., & Tang, T. (2007). Modeling of electron mobility in gated silicon nanowires at room temperature: Surface roughness scattering, dielectric screening, and band nonparabolicity. *Journal of Applied Physics*, *102*(8). https://doi.org/10.1063/1.2802586

32. T. B. Boykin, G. Klimeck, and F. Oyafuso, "Valence band effective-mass expressions in the Sp3d5s∗ empirical tight-binding model applied to a Si and Ge parametrization," Phys. Rev. B, Condens. Matter, vol. 69, no. 11, p. 115 201, Mar. 2004.

33. Martin, M. J., Gonzalez, T., Pardo, D., & Velezquez, J. E. (1994). One-dimensional Monte Carlo analysis of electron transport in sub-micrometer silicon structures. *Semiconductor Science and Technology*, *9*(7), 1316–1323. https://doi.org/10.1088/0268-1242/9/7/004

34. Ashraf, N. S. (2024). Recalculation of Intrinsic Carrier Concentration in Silicon at T = 300 K in Presence of Degenerate Doping. *Silicon*, *16*(1), 435–439. https://doi.org/10.1007/s12633-023-02674-2